SCIENCE CHINA
Earth Sciences

•ARTICLE•

June 2025 Vol.68 No.6: 1937–1959
https://doi.org/10.1007/s11430-024-1561-y

Climate evolution and its driving factors in the Tethys Sea region during the Cenozoic

Jiangbo MENG[1,2], Jiagang ZHAO[1,2], Linlin CHEN[3], Paul J. VALDES[3], Alex FARNSWORTH[3], Svetlana POPOVA[4], Mine Sezgül KAYSERI-ÖZER[5], Gaurav SRIVASTAVA[6], Jian HUANG[1], Tao SU[1,7,8], Zhekun ZHOU[1] & Shufeng LI[1*]

[1]*State Key Laboratory of Plant Diversity and Specialty Crops, Xishuangbanna Tropical Botanical Garden, Chinese Academy of Sciences, Mengla 666303, China*
[2]*University of Chinese Academy of Sciences, Beijing 100049, China*
[3]*School of Geographical Sciences, University of Bristol, Bristol BS8 1SS, UK*
[4]*Komarov Botanical Institute, Russian Academy of Sciences, Saint Petersburg 197022, Russia*
[5]*Institute of Marine Science and Technology, Dokuz Eylül University, Balçova-İzmir 35340, Türkiye*
[6]*Birbal Sahni Institute of Palaeosciences, Lucknow 226007, India*
[7]*Key Laboratory of Deep-time Geography and Environment Reconstruction and Applications of Ministry of Natural Resources, Chengdu University of Technology, Chengdu 610059, China*
[8]*State Key Laboratory of Oil and Gas Reservoir Geology and Exploitation & Institute of Sedimentary Geology, Chengdu University of Technology, Chengdu 610059, China*

Received August 12, 2024; revised March 27, 2025; accepted April 3, 2025; published online May 20, 2025

Abstract The transgression and regression of the Tethys Sea profoundly influenced the environment and biodiversity patterns of Eurasia, which had implications for global climate dynamics by altering the land-sea distribution and the broader moisture transport scheme. Despite its importance, few comprehensive studies have integrated fossil data and climate modeling to explore the climate evolution in the Tethys Sea region during the Cenozoic. In this paper, we reconstruct 10 climate parameters using macrofossil flora from 363 sites across the Tethys Sea region throughout the Cenozoic, and we compare these reconstructions with simulations from the Hadley Center Coupled Model (HadCM3). Additionally, we propose a new Mediterranean Climate Index (MCI), which combines precipitation and temperature, to analyze the evolution of the Mediterranean climate. Our results indicate that the climate in the Tethys Sea region gradually changed from predominantly tropical and subtropical conditions during the Paleogene to a warm temperate and cold temperate climate in the Neogene-Quaternary. The distribution pattern of the coldest month mean surface air temperature (CMMT) changed from a predominantly zonal pattern in the Paleogene to a topographically influenced distribution in the eastern and central Tethys regions since the Neogene. The precipitation patterns in the Tethys Sea region exhibited significant fluctuations. In the western Tethys region, the summer precipitation experienced increased variability, while the winter precipitation decreased slightly. The central Tethys region became significantly drier due to sea regression and mountain uplift. Both the summer and winter precipitation increased markedly in the eastern Tethys region with the development of the Tibetan Plateau. From the Eocene to the early Oligocene, the Mediterranean climate prevailed in Central Asia and Europe, but its extent contracted sharply during the Miocene, primarily due to the decrease in the summer precipitation. The Oligocene-Early Miocene was a critical period for climate evolution in the Tethys Sea region, which was driven by changes in the land-sea distribution, topographic evolution, and global CO_2 concentration. The results of this study provide a crucial reference for exploring the evolution of ecosystems and species diversity in Eurasia driven by climate change since the Cenozoic.

* Corresponding author (email: lisf@xtbg.org.cn)

Keywords Tethys Sea, Cenozoic, Paleoclimate, Plant fossils, Climate modeling

Citation: Meng J, Zhao J, Chen L, Valdes P J, Farnsworth A, Popova S, Kayseri-Özer M S, Srivastava G, Huang J, Su T, Zhou Z, Li S. 2025. Climate evolution and its driving factors in the Tethys Sea region during the Cenozoic. Science China Earth Sciences, 68(6): 1937–1959, https://doi.org/10.1007/s11430-024-1561-y

1. Introduction

A series of significant geological events occurred in the Cenozoic, reshaping the Earth's climate and biogeography, including the closure of the Neotethys Ocean, fluctuations in the global sea level, the formation of the Alpine-Himalayan orogenic belt, and the development of the Tibetan Plateau (Li, 1999; Zheng and Yao, 2006; Zhang et al., 2007; Sun et al., 2013; Zheng et al., 2014; Deng and Ding, 2015; Wu et al., 2020; Westerhold et al., 2020; Zhu et al., 2022; Sun et al., 2023). The Tethys Sea, as the western remnant of the closing Neotethys Ocean, was situated between the Eurasian Plate and the African-Arabian Plate, and it linked the ancient Atlantic and polar oceans. Over time, it evolved into the present-day Mediterranean Sea (Sun et al., 2013; Wu et al., 2020; Zhu et al., 2022). As one of the major geological events in the Cenozoic, the transgression and regression of the Tethys Sea significantly impacted the climate and biodiversity pattern in Eurasia and the broader global climate by altering the land-sea distribution and moisture transport (Sun et al., 2013). The rapid northward drift of the African-Arabian and Indian plates and their collision with the Eurasian plate led to the closure of the Tethys Sea. This tectonic activity not only reconfigured the regional land-sea distribution but also altered the dynamics of the key straits, impacting the regional vapor sources and disrupting oceanic salt and heat exchange through altered currents. These changes created new opportunities for the exchange and dispersal of flora and fauna (Hamon et al., 2013; Liu et al., 2018; Sun et al., 2021a; Zhao Z et al., 2022; Sun et al., 2024). The climatic effects caused by major geological events can directly or indirectly drive the evolution of vegetation and biodiversity (Jin et al., 2003). Therefore, studying the impact of the closure of the Cenozoic Tethys Sea on the climatic evolution in coastal regions provides a foundation for gaining a deeper understanding of the evolution of ecosystems and biodiversity in this region.

In recent years, the importance of the evolution of the Tethys Sea has garnered much attention, and researchers have conducted a series of studies on this subject (Wu et al., 2020; Zhu et al., 2022). Although there is considerable debate regarding the extent of the Tethys Sea in the Cenozoic and the timing of its retreat and closure, the results of numerous studies generally indicate that the retreat of the Tethys Sea in the Cenozoic was a complex and gradual evolutionary process. Recent geological evidence suggests that the Indian Plate collided with Eurasia at around 65–63 Ma (Ding et al., 2017) and that the Tethys Sea retreated from the southern margin of the Tibetan Plateau by the late Eocene. Influenced by global sea-level fluctuations and tectonic compression, and following several cycles of transgression and regression, the Tethys Sea ultimately withdrew from the Tarim and Tajik Basins during the late Eocene (around 47 Ma and 38.6 Ma, respectively) (Sun and Jiang, 2013; Sun et al., 2016, 2020). Influenced by the collision between the African-Arabian Plate and the Iranian Plate (35–20 Ma), seawater retreated from central Iran during the Early Miocene at 16.8 Ma (Sun et al., 2021b), and the Tethyan seaway in the northwestern Iranian Plateau permanently closed in two phases, culminating at 12.8 Ma (Sun et al., 2021a). Currently, a significant amount of research has focused on reconstructing the paleogeography of the Tethys Sea in the Cenozoic, but the effects of its geological evolution on the climate of this region remain poorly understood (Wu et al., 2020).

The Cenozoic was characterized by global cooling, the retreat of the Tethys Sea, and the development of the Tibetan Plateau, all of which profoundly influenced the climate in the Tethys region. Geological evidence suggests that aridification in Central Asia began in the late Eocene, which was potentially linked to global climate and sea level changes. By the early Oligocene, the vegetation in the region had begun to adapt to the increasing degree of aridity. Following the complete withdrawal of the Tethys Sea from the Iranian Plateau in the Middle Miocene, the arid conditions intensified, leading to a shift in the vegetation types toward open steppe and savanna landscapes (Bruch and Zhilin, 2007; Cai et al., 2012; Bosboom et al., 2014; Carrapa et al., 2015; Wang et al., 2016; Popova et al., 2017; Sun et al., 2020, 2021b). Extensive research has also focused on East Asia's climatic evolution. For example, the differentiated uplift of the Tibetan Plateau led to a shift in the atmospheric circulation from a planetary wind system during the Paleogene to a monsoonal system in the Neogene, and the Oligocene-Miocene transition was a key period of environmental change in East Asia. The Southeast Asian monsoon may have developed during the Oligocene, likely driven by the contraction of the Tethys Sea, which established a strong land-sea contrast across the Eurasian continent, rather than the development of the Tibetan Plateau (Liu et al., 1998; Li, 1999; An et al., 2006; Guo, 2017). Paleobotanical evidence suggests that the middle and low latitude regions of Europe

had a warm and humid climate overall during the Paleogene-Miocene (Velitzelos et al., 2014; Denk et al., 2022; Postigo-Mijarra et al., 2022). After the Middle Miocene, the climate gradually became drier and colder. Following the Messinian salinity crisis and the Zanclean flood, the ancient Mediterranean Sea formed (Krijgsman et al., 1999; Duggen et al., 2003; Garcia-Castellanos et al., 2009; Garcia-Castellanos and Villaseñor, 2011; Hernández-Molina et al., 2014), and the morden Mediterranean climate may have formed during the Pliocene (Suc, 1984).

The morden Mediterranean climate, characterized by its unique seasonal patterns of rainfall and temperature, is a subtropical dry-summer climate that is governed alternately by the westerlies and subtropical high-pressure zones. It is characterized by mild, rainy winters and hot, dry summers (Deitch et al., 2017). Köppen classified it as Cs type, a temperate climate type that exists on the west coasts of continents at latitudes of 30°–40°. In this climate, the coldest month mean surface air temperature (CMMT) ranges from −3°C to 18°C, and the precipitation in the driest month in summer is less than 30 mm, which is less than one-third of the precipitation in the wettest month in winter (Kottek et al., 2006; Kutiel and Türkeş, 2017). Currently, there are five major Mediterranean climate regions in the world: Southwest Australia, the Cape Region of South Africa, the Mediterranean Basin, California, and Central Chile (Rundel et al., 2016; Deitch et al., 2017). The complex topography of the Mediterranean Sea region significantly influences both the oceanic and atmospheric circulation, making the Mediterranean climate particularly distinctive in this area (Lionello et al., 2006). The evolution of the Mediterranean climate is a significant but complex scientific issue, and there is ongoing debate due to the limited availability of terrestrial evidence. Paleontological and geological evidence shows that the Tethys region experienced a warm and humid tropical and subtropical climate during the Paleogene (Aleksandrova et al., 1987; Barrón et al., 2010; Serkan Akkiraz et al., 2022). Palynological records suggest that summer drought first occurred in the Northwest Mediterranean during the late Pliocene (3.2 Ma) (Suc, 1984). Further studies indicate that the Mediterranean climate conditions began on the Iberian Peninsula in the late Pliocene to early Pleistocene, which resulted in the gradual emergence of Mediterranean-type plant taxa (Postigo-Mijarra et al., 2009; Barrón et al., 2010). During the Middle Miocene to Pliocene, C4 plants expanded, but C3 plants remained widespread in the Mediterranean region, possibly due to the fact that the seasonal drought limited C4 plant growth in this region (Edwards et al., 2010). Zhao et al. (2023) reconstructed the uplift history in the middle and late Eocene in the Markam Basin in Xizang using geochemical evidence and modeling, and they concluded that the southeast margin of Xizang experienced a Mediterranean-type climate during the late Eocene. However, this conclusion lacks sufficient plant fossil evidence, highlighting the need for further cross-validation of the evolution of the Mediterranean climate.

Plant fossils are reliable proxies for paleoclimate reconstruction (Su et al., 2019, 2020; Huang et al., 2020; Zhao J G et al., 2022). Since the 20th century, numerous plant fossil taxa have been documented (Gregor, 1990; Bozukov et al., 2009, 2021; Postigo-Mijarra et al., 2009; Hably, 2010, 2020; Bertini and Martinetto, 2011; Collinson et al., 2012; Erdei et al., 2012, 2022; Mach et al., 2014; Teodoridis et al., 2015; Worobiec et al., 2015; Denk et al., 2017, 2021, 2022; Kvaček and Bubík, 2016; Kvaček et al., 2018; Macaluso et al., 2018; Kunzmann et al., 2019; Worobiec and Worobiec, 2019; Erdei and Wilde, 2020; Jolly-Saad et al., 2020; Tanrattana et al., 2020; Bubík et al., 2022; Kafetzidou et al., 2022; Altolaguirre et al., 2023). These studies have been instrumental in collecting and analyzing fossil data, which can be employed to reconstruct regional climates across key geological periods using methods such as the Coexistence Approach (CA), Climate-Leaf Analysis Multivariate Program (CLAMP), and Leaf Margin Analysis (LMA). These findings indicate that the climate in the Tethys region underwent a transition from a humid subtropical climate in the Paleogene, to a warm temperate climate in the Neogene, and finally to a cooler and more arid climate in the Quaternary (Thiel et al., 2012; Velitzelos et al., 2014; Kayseri-Özer, 2017; Tosal et al., 2019, 2021; Zhao J G et al., 2022; Khan et al., 2023). LMA and CLAMP are both based on the application of the correlation between leaf morphology and the environment to reconstruct the paleoclimate. LMA employs a univariate regression equation, which is straightforward and easy to operate, but its accuracy is influenced by the uniformity and abundance of the sampling, making it suitable for reconstructing specific regional climate conditions (Wilf, 1997; Traiser et al., 2005; Su et al., 2010). In comparison, the CLAMP can reconstruct a greater number of climate parameters, but it is affected by the geographic location and climate range of the calibration dataset (Yang et al., 2007, 2011). CA is based on the assumption that plant fossils and modern plants live under similar climatic conditions (Mosbrugger and Utescher, 1997), and it reconstructs paleoclimate using the Nearest Living Relatives (NLRs), making it applicable to various types of plant fossils (Utescher et al., 2014).

Research on paleoclimate evolution, characterized by long-term and large-scale processes, can benefit significantly from numerical simulations, which complement observational research (Liu, 1993). The effects of the aridification of Central Asia and the development of the Tibetan Plateau on the climate in East Asia have been studied using model simulations (Ramstein et al., 1997; Zhang et al., 2007, 2021; Li et al., 2018, 2021). The sensitivity tests conducted by Ramstein et al. (1997) highlight the crucial influences of

topographic changes, plate movements, and changes in the land-sea distribution on the Eurasian climate since 30 Ma. Zhang et al. (2007, 2021) utilized model simulations to compare the effects of the development of the Tibetan Plateau, the retreat of the Paratethys Sea, and global cooling on the East Asian Summer Monsoon climate. Similarly, Li et al. (2018) investigated climate differences across various Eurasian regions during the Oligocene, and they found that the model-simulated variations in the seasonal temperature in the middle to high latitude regions were significantly greater than those reconstructed from fossil data. By comparing model simulations with fossil records, researchers can evaluate their congruence and explore the driving factors behind climate and ecosystem changes (Ding and Xiong, 2006). However, few comprehensive studies that integrate fossil records and models, particularly those focused on long-term, large-scale Cenozoic climate evolution in the coastal region of the Tethys Sea, have been conducted. Consequently, the driving factors of the climate evolution in these areas are not yet fully understood.

In this study, the Hadley Center Coupled Model version 3 (HadCM3) was employed to simulate the paleoclimate in the Tethys Sea region under the geological events related to the retreat of the Tethys Sea in the Cenozoic. This was coupled with evidence from 363 plant fossil sites to quantitatively reconstruct the paleoclimate using the Joint Probability Density Functions (JPDFs) method. Through a comprehensive comparative analysis of the numerical simulations and paleoclimate reconstructions, we aimed to elucidate the evolution of the climate in the coastal region of the Tethys Sea across different geological periods in the Cenozoic. Furthermore, we aimed to identify the driving factors behind the climate changes in the middle and low latitude regions along the coast of the Tethys Sea while considering the significant transformations of the Earth's systems since the Cenozoic.

2. Materials and methods

2.1 Collection of paleobotanical data

In this study, we obtained fossil data from the Paleobiology database (PBDB, https://paleobiodb.org/classic), Cenozoic angiosperm database (CAD; Xing et al., 2016), Paleoecology Database (PEDB, http://pd.xtbg.ac.cn/) established by the Paleoecology Research Group of Xishuangbanna Tropical Botanical Garden, Chinese Academy of Sciences, and related literature. We also collected important information such as the modern latitude and longitude, age, dating method, and plant fossil taxa of the fossil sites within the modern latitude and longitude ranges of −8°–110°E and 24°–50°N. Due to the limitations of each database, there were gaps in the information for some fossil sites. To address this, we cross-referenced the data from these databases with a large volume of paleoflora-related literature. We deleted the duplicate fossil sites in the three databases, added the missing fossil sites, and updated and supplemented the longitude and latitude of the fossil sites and dating methods. Utilizing the paleobotanical database (PALAEOFLORA, https://www2.geo.uni-bonn.de/Palaeoflora/palaeoflora.html) and the Plants of the World Online (https://powo.science.kew.org/), the NLRs of the fossils and their family, genus, and species information were carefully checked. Ultimately, a total of 363 macrofossil plant sites in the Tethys Sea region in the Cenozoic were integrated (Figure 1, Appendix 1, https://link.springer.com), establishing a comprehensive paleoflora database for the Tethys Sea region in the Cenozoic.

To facilitate comparison between the reconstruction and simulation results, we used the "Reconstruct" function in the R package "rgplates" and the Gplates "SETON2012" model (https://gwsdoc.gplates.org/) to convert the modern coordinates of the fossil sites into their corresponding paleocoordinates. The median value of the fossil age range was used as the specific age value for this conversion.

To conduct a detailed analysis of the climate history and its driving factors across different regions of the Tethys Sea, the study area (−8°–110°E, 24°–50°N) was divided into three regions (Figure 1): the western Tethys (−10°–28°E, 35°–50°N, primarily including the Iberian Peninsula, Apennine Peninsula, Balkan Peninsula, France, and Germany), central Tethys (28°–73°E, 24°–50°N, primarily in Central Asia, including Türkiye and Kazakhstan), and eastern Tethys (73°–110°E, 15°–40°N, mainly including the Tibetan Plateau, surrounding areas in Southwest China, the Indian Peninsula, and the Indochina Peninsula region). These region names are not proper nouns but are used here to denote distinct areas delineated for the purposes of this study.

2.2 Quantitative reconstruction of the paleoclimate

Based on the collected paleobotanical data, in this study, we employed the JPDFs method (Willard et al., 2019) to reconstruct the paleoclimate in the Tethys Sea region during the Cenozoic. This method is similar in principle to the Bioclimatic Analysis (BA) method (Li et al., 2015) and the CA (Mosbrugger and Utescher, 1997). The difference lies in the fact that the JPDFs enhance the reliability of reconstructing paleoclimate variables through statistical methods using probability density functions. It assumes that the distribution area of a taxon follows a certain probability density distribution (e.g., normal distribution), meaning that most species are distributed within the climate range of their higher probability density. Thus, by calculating the joint probability density of multiple species, the optimal climate estimates for these species can be obtained. Initially, the modern distribution points of the NLRs are obtained from the

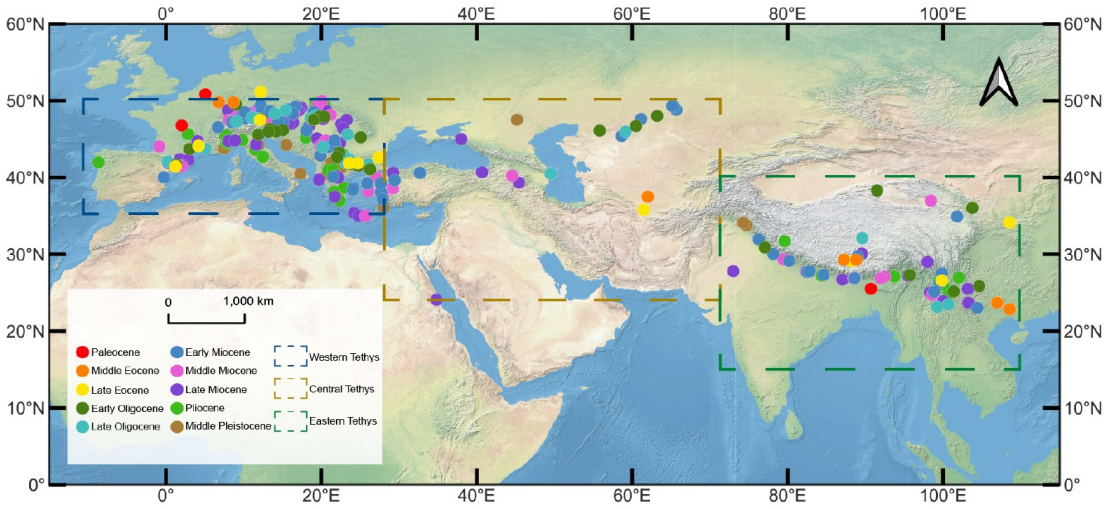

Figure 1 Distribution of plant fossil sites in the Tethys Sea region during the Cenozoic.

Global Biodiversity Information Facility (GBIF, https://www.gbif.org/), artificially cultivated records are excluded, and the distribution points are processed using a sparsity filter (accuracy of ~5 km). Subsequently, climate data corresponding to these distribution points are extracted from the Climatologies at high resolution for the Earth's land surface areas (CHELSA) climate database. The JPDFs method enables calculation of the most probable paleoclimate values, as well as estimation of interval ranges (5%–95%).

During the process of identifying the NLRs, certain plant groups with limited significance for paleoclimate reconstruction were excluded, such as extinct plant groups, aquatic plant groups, and ferns. Furthermore, to enhance the resolution and reliability of the reconstruction results (Utescher et al., 2000; Bruch and Zhilin, 2007; Serkan Akkiraz et al., 2022), fossil sites with fewer than 10 plant fossil records were also excluded. The current climate data for the species distribution were obtained from the CHELSA database. CHELSA is a high-resolution dataset (30′, ~1 km) derived using a dynamic downscaling method, which is highly reliable and accurate under complex topographical conditions. This dataset provides a range of climatic indicators, including temperature, precipitation, humidity, wind speed, and cloud cover, which are crucial for understanding climate characteristics, conducting environmental and ecological research, and predicting future climate changes (Karger et al., 2017). In this study, we quantitatively reconstructed 10 common climatic indicators, namely, the mean annual temperature (MAT, Bio1), warmest month mean surface air temperature (WMMT), CMMT, mean temperature in wettest quarter (MTWetQ, Bio8), mean temperature in driest quarter (MTDryQ, Bio9), mean temperature in warmest quarter (MTWQ, Bio10), mean temperature in coldest quarter (MTCQ, Bio11), mean annual precipitation (MAP, Bio12), precipitation in warmest quarter (PWQ, Bio18), and precipitation in coldest quarter (PCQ, Bio19), to reconstruct the paleoclimate of the coastal region of the Tethys Sea during the Cenozoic (Appendix 3).

2.3 Analysis of Mediterranean climate

Given the limitations inherent in paleoclimate reconstruction, certain climatic indices used to describe the current Mediterranean climate are not entirely applicable in quantitative analysis of its evolution. To analyze seasonal precipitation differences, in this study, we primarily introduced two indices based on the definition of the Mediterranean climate proposed by Deitch et al. (2017): the percentage of summer precipitation and the percentage of winter precipitation. These indices rely on the precipitation data for the 3 summer months and the 6 coldest months, respectively. Since it is challenging to quantitatively reconstruct the precipitation in the coldest 6 months in paleoclimate reconstruction, the PCQ (the precipitation in the 3 coldest months) was used in the calculations. The Mediterranean Climate Index (MCI) is an index used to measure the seasonal differences in precipitation (Kutiel and Türkeş, 2017), generally assessed as the difference between the PCQ (Bio19) and PWQ (Bio18). Kutiel and Trigo (2014) modified the Köppen classification of the Mediterranean climate, stating that the PCQ (DJF) should be three times the PWQ (JJA). Additionally, the CMMT is also an important indicator for determining the type of Mediterranean climate, and it typically ranges from −3°C to 18°C for Mediterranean climates (Kottek et al., 2006). To explore the evolution of the Mediterranean climate, we employed the "LookupCZ" function in the R package "kgc" to obtain the geographic coordinates of the global Mediterranean climate regions, and we extracted the CMMT, PCQ, and PWQ based on the CHELSA climate data. The precipitation dif-

ference between the winter and summer (Pws) can be calculated as follows:

$$\mathrm{Pws} = \log(\mathrm{Bio19}+1) - \log[(\mathrm{Bio18}+1)\times 3]. \quad (1)$$

To avoid infinite values, 1 is added to the values of both Bio19 and Bio18, transforming log(x) into log(x+1). This transformation method is a commonly used statistical technique for data conversion. It slightly alters the data, but the addition of 1 has a minimal impact and does not generally affect the overall distribution and relative differences of the data. Based on the probability distributions of CMMT and Pws (Appendix 4), we developed the following equation for calculating the MCI:

$$\mathrm{MCI} = e^{-\frac{(\mathrm{CMMT}-7.5)^2}{2\sigma^2\mathrm{CMMT}}} \times e^{-\frac{(\mathrm{Pws}-0)^2}{2\sigma^2\mathrm{Pws}}}, \quad (2)$$

where 7.5 and 0 are the expected values of the CMMT and Pws, respectively, based on the calculations for the Mediterranean climate (Appendix 4). The MCI combines the probability distribution patterns of two independent measurements, the CMMT and Pws, and indicates how much they deviate from their expected values. For each measurement, assuming a normal distribution, they represent the deviation from the expected value. The first factor in eq. (2) measures the degree to which the CMMT value deviates from 7.5. The smaller the deviation is, the closer the value of this factor is to 1; while larger deviations bring it closer to 0. The second factor in eq. (2) measures the degree to which the Pws value deviates from 0; similarly, smaller deviations bring this factor closer to 1, and larger deviations bring it closer to 0. By multiplying these two factors, the MCI comprehensively considers the degree to which both of these independent measurements deviate from their expected values. The value of the MCI is between 0 and 1, with higher values indicating that the CMMT and Pws are closer to their expected values, indicating greater similarity to the Mediterranean climate.

Additionally, based on the Mediterranean climate values obtained from the CHELSA database, the Mediterranean climate we established needs to meet three conditions: (1) Bio18 < 80 mm, (2) Bio19 > 120 mm, and (3) −3°C < CMMT < 18°C. Based on the modern climate data from the CHELSA database, we calculated the modern MCI and the distribution area of the Mediterranean climate (Appendix 4), which generally aligns with the current distribution of the Mediterranean climate (Mediterranean (Summer-Dry) Climates, https://www.pacificbulbsociety.org/pbswiki/index.php/DrySummer-Climates), with only slight differences along the Apennine Peninsula and the coast of the Balkan Peninsula.

By integrating the MCI with the aforementioned three climatic factors, we conducted a comprehensive analysis of the evolution of the Mediterranean climate in the Tethys Sea region during the Cenozoic based on fossil and climate simulation results.

2.4 Numerical simulations of paleoclimate

In this study, the HadCM3 developed by the University of Bristol, UK, was used to simulate the paleoclimate over 10 geological periods from the Paleocene to the Quaternary (Appendix 2) (Valdes et al., 2021; Fenton et al., 2023). The horizontal resolution of the atmospheric model is 3.75° (longitude)×2.5°(latitude), and it has 19 layers. The ocean model has a resolution of 3.75°(longitude)×2.5°(latitude) and has 20 layers (Valdes et al., 2017). The model simulates the climate throughout the geological period by setting boundary conditions such as the solar constant, atmospheric CO_2 concentration, land-sea boundary, topography, soil and vegetation types, and physical changes (Valdes et al., 2017, 2021). The land-sea boundaries, elevations, and ice sheets were set based on the paleogeographic data of Scotese (2016). The CO_2 concentrations were revised and set based on the work of Foster et al. (2017). Given that most of the Quaternary fossil sites are concentrated in the Pleistocene epoch, the mean values of the Middle Pleistocene Transition (MPT; 1200–700 K) climate simulations were used for comparison (Sun et al., 2019). The climate tests were run for 1000 years in each period, ensuring that both the surface and deep ocean were in dynamic equilibrium and that there was no energy imbalance at the top of the atmosphere (Valdes et al., 2021). When the model reached equilibrium, the climate average of the last 100 years was analyzed as the simulation result.

In addition, based on Sagoo et al. (2013) and Kiehl and Shields (2013), the version of the HadCM3 climate model used in this study was modified for parameters such as cloud condensation nuclei density and cloud droplet effective radius, thereby increasing the temperature in the high latitude region, which is often underestimated, but this did not significantly change the temperature in the tropical region. The simulation results are in better agreement with the observed results (Fenton et al., 2023). The model adopts the land surface exchange system of the Met Office Surface Exchange Scheme (MOSES2.1) (Cox et al., 2000) and the Top-down Representation of Interactive Foliage and Flora Including Dynamics (TRIFFID), to conduct a coupled simulation of the vegetation-climate interaction (Cox et al., 1998; Cox, 2001). The model generates land boundaries for topographic data through high-resolution resampling and neighborhood analysis. Initially, the original topographic data are gridded, enhancing its resolution to 5′. Subsequently, the "focal" function in the R package "terra" is utilized to calculate the proportion of land around each grid, with a threshold set to distinguish land from ocean, thereby producing preliminary land boundaries. Finally, these boundaries are further refined by integrating global vector land data, making them suitable for climate and topographic analysis.

3. Results

3.1 Spatial analysis of paleoclimate

3.1.1 Spatial analysis of temperature

Overall, the MAT (Figure 2), WMMT (Figure 3), and CMMT (Figure 4) along the Tethys Sea region, which were quantitatively reconstructed from fossil flora, are generally consistent with the trends simulated using the model. However, during the Paleocene and Eocene, the reconstructed MAT is slightly lower than the simulation results. Similarly, the reconstructed WMMT is also lower than the simulation result overall, while the reconstructed CMMT is significantly higher on the southern margin of the Tibetan Plateau (Figure 4b–4e).

From the Paleocene to the late Eocene, the MAT and CMMT in the Tethys Sea region were characterized by a zonal distribution, and the temperature decreased from low latitudes to high latitudes. However, with the development of the Tibetan Plateau and the westward retreat of the Tethys Sea in the late Eocene, the distributions of the MAT and CMMT in the eastern and central Tethys began to shift toward a topography-dominant type, while the western Tethys was still dominated by a zonal type distribution (Figures 2 and 4). In the western Tethys (Figure 4), the CMMT consistently ranged from −3°C to 18°C, with minimal fluctuations, resembling the temperature patterns of the modern Mediterranean climate. The distribution pattern of the WMMT differed from that of the MAT and the CMMT, exhibiting a decreasing trend centered on the mid-latitude region of the Tethys Sea. In the late Eocene, on the Tibetan Plateau, the WMMT began to exhibit a topography-dominated distribution pattern (Figure 3h).

3.1.2 Spatial analysis of precipitation

In general, the reconstructed precipitation in the Tethys Sea region during the Cenozoic is consistent with the trend of the numerical simulation, but there are obvious regional differences (Figures 5–7). Specifically, the reconstructed PCQ on the Tibetan Plateau is higher than the simulated precipitation (Figure 7).

The spatial distribution of precipitation is characterized by a pattern of drought at mid-latitudes in Central Asia, with gradually increasing precipitation in the surrounding areas. This arid region expanded continuously from the Paleocene to the Miocene, slightly contracted after the Pliocene, and then stabilized. In the middle and high latitude regions, the precipitation decreased from the western coast of the continent to the east, particularly in the distribution of the PCQ, which was the most pronounced. The mid-latitude arid regions continued to expand northeastward, while the precipitation in southeast China began to increase in the Early Miocene (Figure 7). On the southern Tibetan Plateau and in southeast China, the MAP and PWQ gradually increased from the late Eocene onward (Figures 5h and 6h). In the western Tethys region, the PCQ decreased slightly during the Cenozoic (Figure 7), while the PWQ exhibited a fluctuating increasing trend, and the areas receiving less than 80 mm of PWQ expanded during the Paleocene-Eocene (Figure 6h–6j). Since the Oligocene, the extent of this region has shrunk. In particular, precipitation has increased in the middle and high latitude regions.

According to the simulation results of the distribution of the Mediterranean climate during the Cenozoic, the Mediterranean climate types were most widespread in the western and central Tethys regions during the Eocene-early Oligocene (Figure 8g–8i). However, the distribution of the Mediterranean climate sharply decreased in the Miocene (Figure 8c–8e). It became sporadically located around the Black Sea and the Paleo-Mediterranean and then somewhat recovered in the Pliocene (Figure 8b). By the middle Pleistocene, the distribution largely aligned with the modern Mediterranean climate distribution in Europe (Figure 8a). In the western Tethys region, the PCQ was generally greater than 120 mm during the Cenozoic, while the trend of the PWQ (Figure 3) was more complex. The areas with less than 80 mm of precipitation expanded from the Paleocene to the Eocene and then shrank in the Oligocene. These areas became primarily concentrated along the eastern coast of the Black Sea and on the southernmost edge of the Iberian Peninsula. By the Pleistocene, this region had expanded, and the simulated range of the Mediterranean climate expanded accordingly. The reconstruction results are largely consistent with the simulation results.

3.2 Temporal analysis of paleoclimate

3.2.1 Temperature variations

The trends of the simulated MAT, WMMT, and CMMT in the western, central, and eastern Tethys regions are largely consistent, and the paleo-temperature trends in the western and central Tethys regions exhibit a higher degree of similarity. In the western Tethys region, the simulated MAT is 16–23°C, the WMMT is 27.5–41.5°C, and the CMMT is 7.5–11°C. In the central Tethys region, the simulated MAT is 18.5–26°C, the WMMT is 31–44°C, and the CMMT is 3–11.5°C. In the eastern Tethys region, the simulated MAT is 15.5–27°C, the WMMT is 23–36.5°C, and the CMMT is 5.8–13.5°C. According to the trends derived from the model simulations, the temperature trends in the Tethys Sea region during the Cenozoic are largely consistent with the global CO_2 concentration trends, showing significant late Paleocene warming and an Eocene-Oligocene transition to cooling. The temperatures in the western and central Tethys regions exhibited fluctuating changes during the Paleocene to Quaternary, with no drastic changes in altitude occurring in these regions. In the western Tethys region, the trend of the pro-

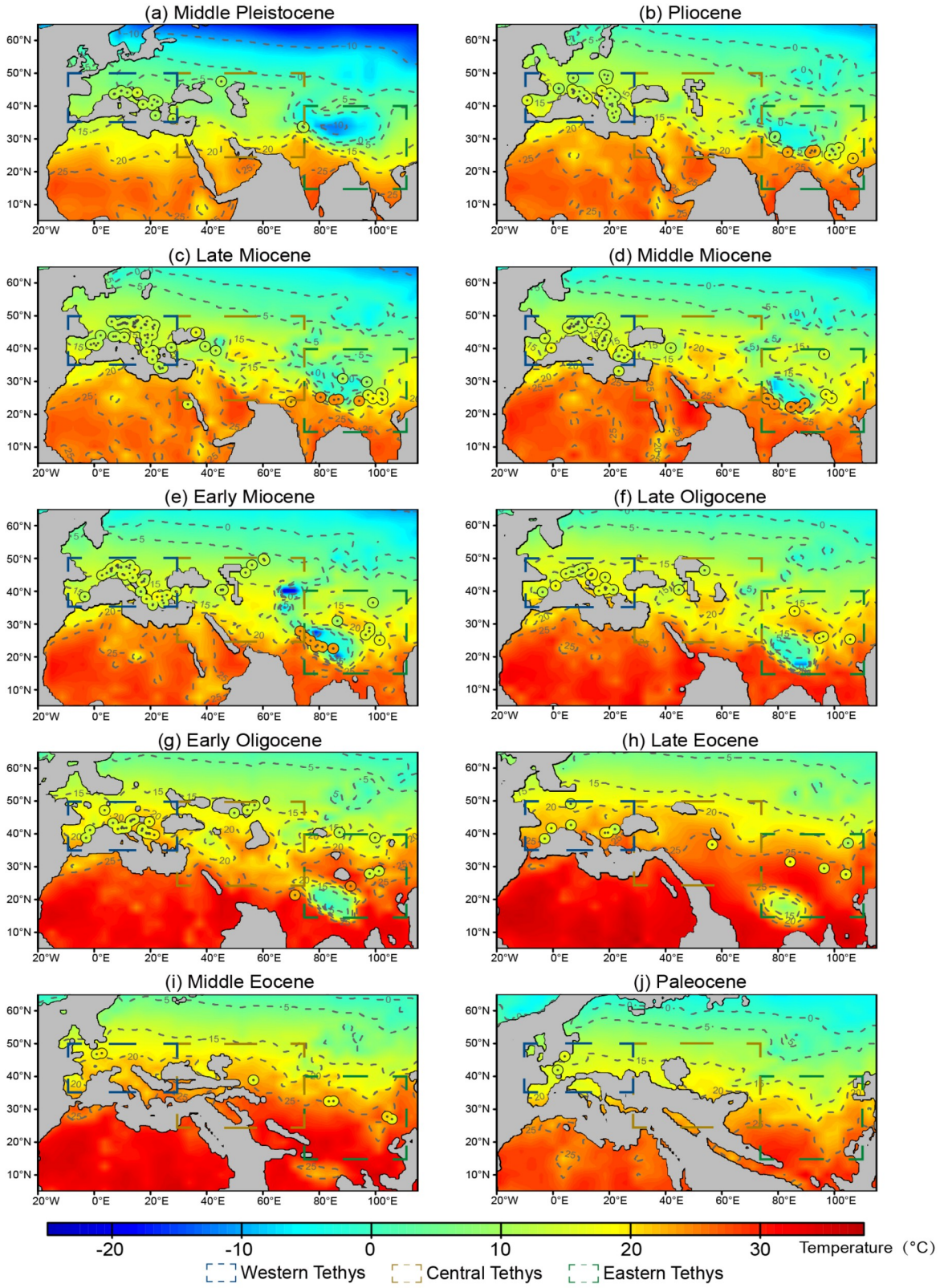

Figure 2 Mean annual temperature (MAT) in the Tethys Sea region during the Cenozoic. The circles represent the MAT reconstructed from fossils, and the background colors represent the MAT from the model simulations. The western Tethys region experienced a warming trend from the Paleocene to the late Eocene, followed by significant cooling starting in the early Oligocene. The central Tethys region experienced a warming trend during the Paleocene-Eocene, during which the landmass rapidly moved northward and the Tethys Sea quickly closed in Central Asia. Subsequently, significant cooling began in the early Oligocene. The eastern Tethys region experienced overall higher temperatures during the Paleocene and Eocene, and significant cooling occurred in the surrounding areas during the late Eocene as the Tibetan Plateau rapidly uplifted.

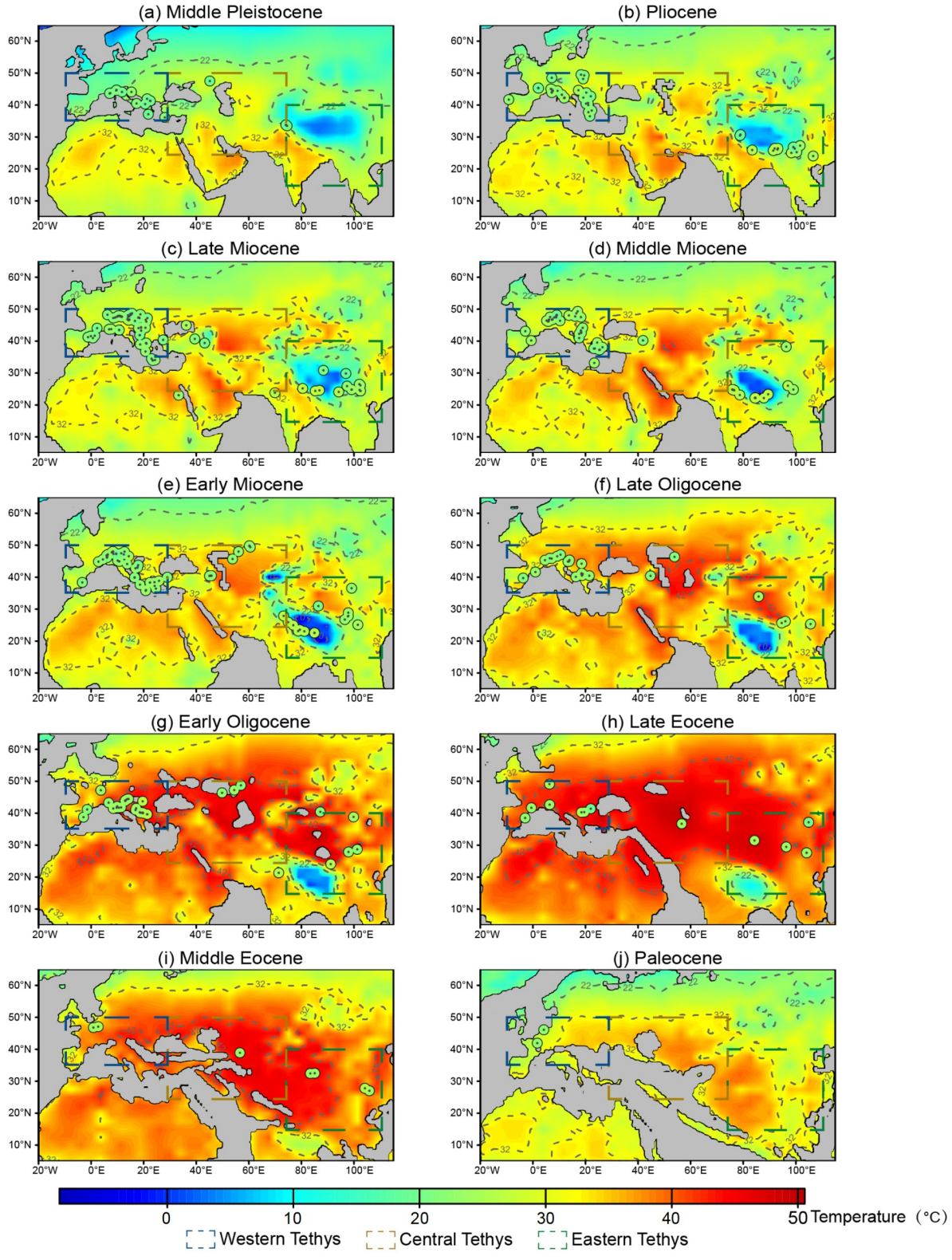

Figure 3 Warmest month mean surface air temperature (WMMT) in the Tethys Sea region during the Cenozoic. The circles represent the WMMT reconstructed from fossils, and the background colors represent the WMMT from the model simulations. The western Tethys region experienced a warming trend from the Paleocene to the late Eocene, followed by significant cooling starting in the early Oligocene. The central Tethys region experienced overall higher temperatures during the Paleocene-Oligocene, with significant cooling beginning in the Early Miocene. The eastern Tethys region experienced a warming trend and overall higher temperatures during the Paleocene and Eocene. A cooling trend emerged as the Tibetan Plateau rapidly uplifted in the late Eocene, and low temperatures occurred in the Tibetan Plateau region from the late Oligocene to the Miocene.

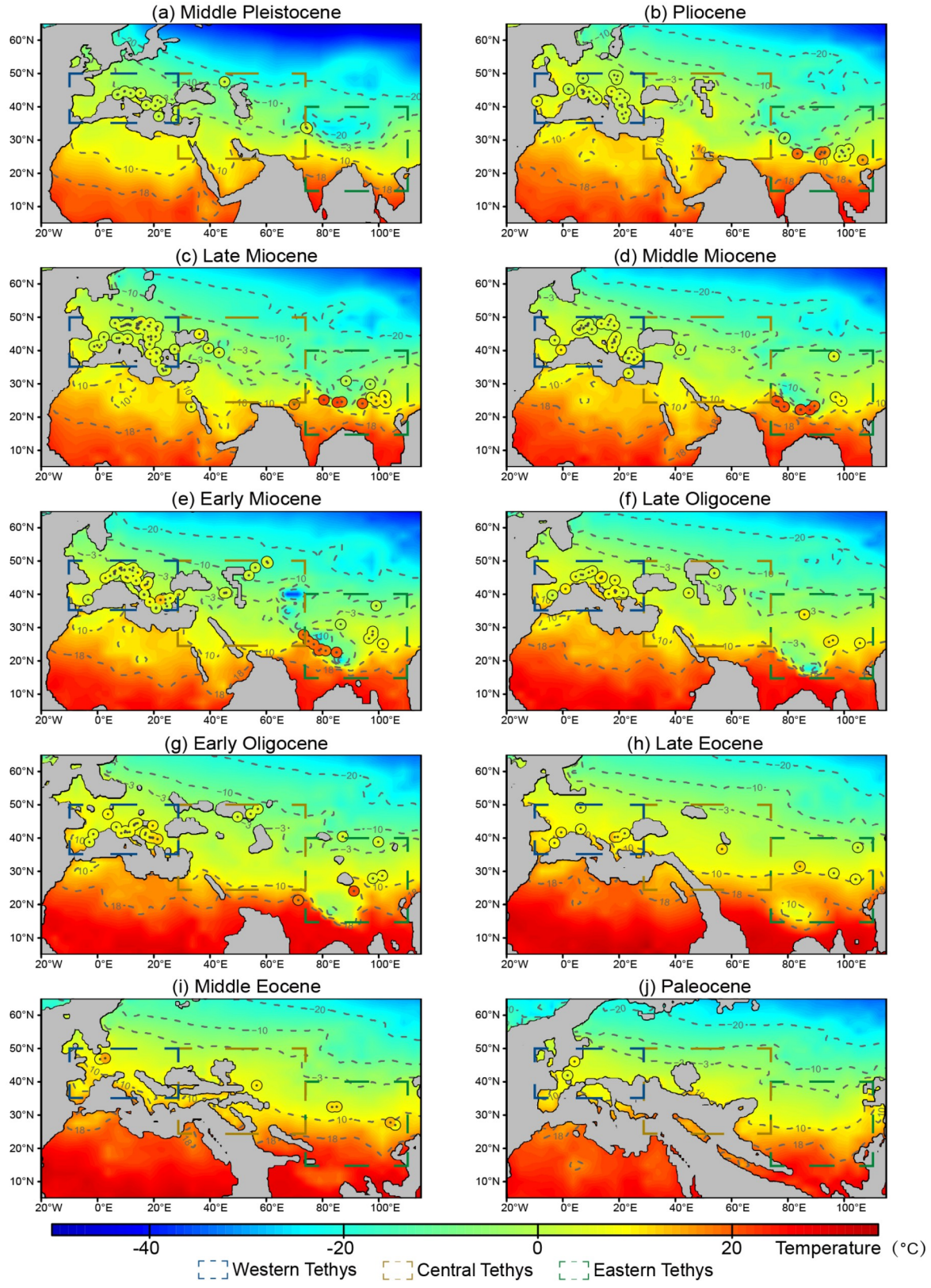

Figure 4 Coldest month mean surface air temperature (CMMT) in the Tethys Sea region during the Cenozoic. The circles represent the CMMT reconstructed from fossils, and the background colors represent the CMMT from the model simulations. The CMMT in the western Tethys region increased slightly during the Paleocene and Eocene, but a gradual cooling trend began in the early Oligocene. The central Tethys region also experienced a warming trend from the Paleocene to the Eocene, followed by gradual cooling starting in the early Oligocene. The eastern Tethys region experienced relatively stable temperatures during the Paleocene and Eocene, but significant cooling occurred in the Tibetan Plateau area and surrounding areas in the early Oligocene.

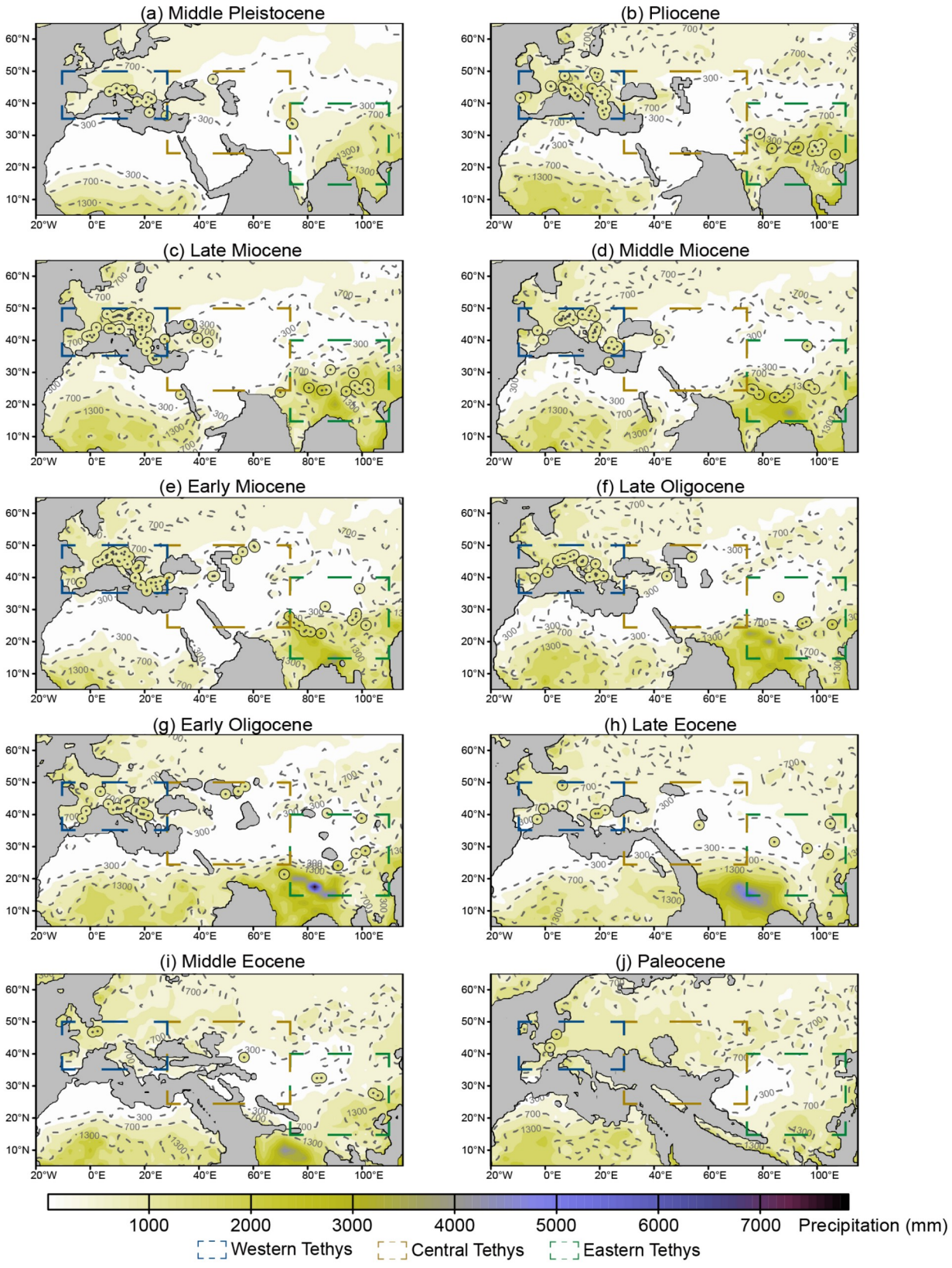

Figure 5 Mean annual precipitation (MAP) in the Tethys Sea region during the Cenozoic. The circles represent the MAP reconstructed from fossils, and the background colors represent the MAP from the model simulations. During the Cenozoic, in the western Tethys region, the MAP did not change significantly, but it experienced a slight decreasing trend overall. In the central Tethys region, the MAP significantly decreased during the middle Eocene, and the arid regions continuously expanded. In the eastern Tethys region, the MAP generally increased as the Indian Plate moved northward.

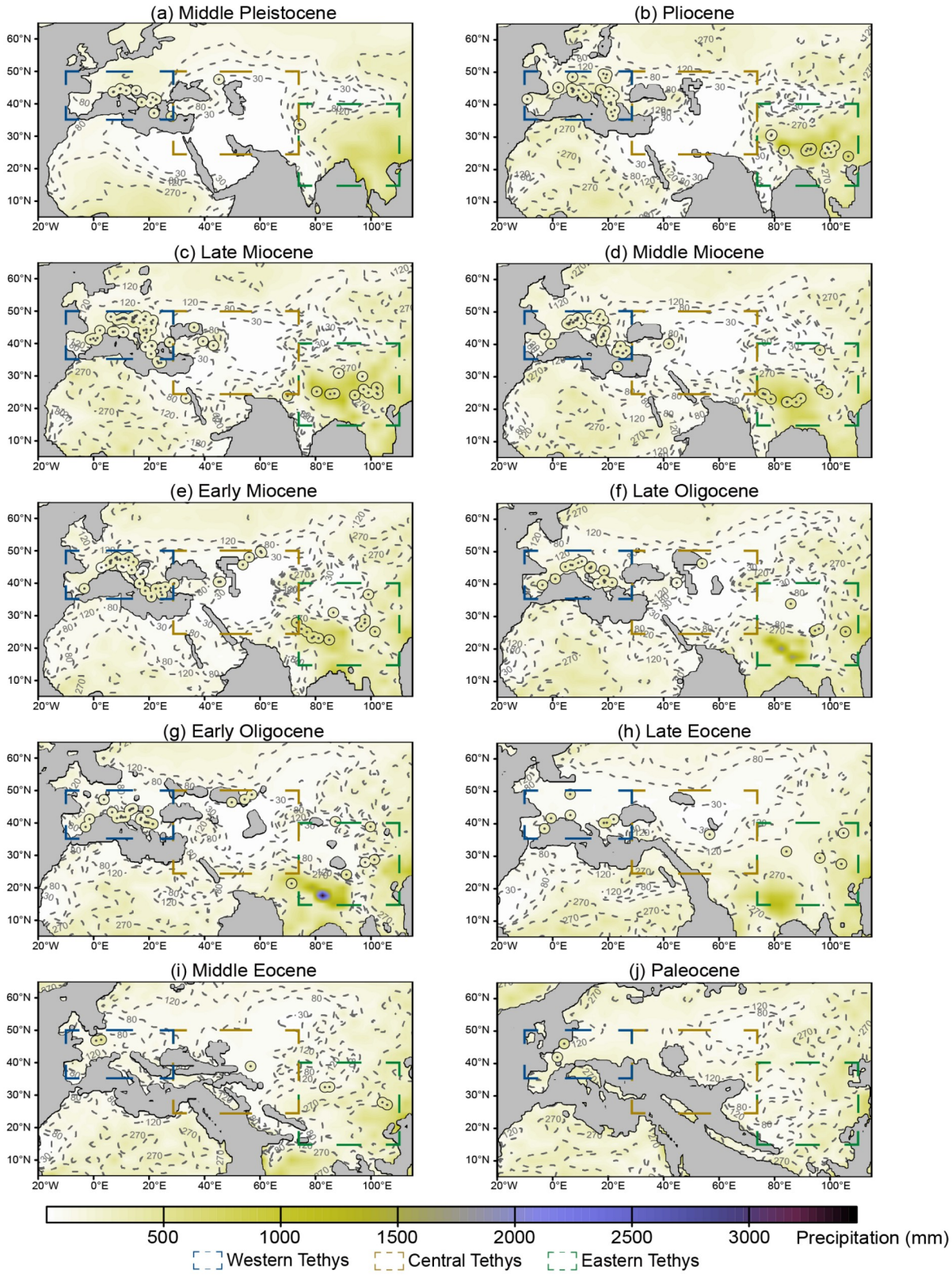

Figure 6 Precipitation in warmest quarter (PWQ) in the Tethys Sea region during the Cenozoic. The circles represent the PWQ reconstructed from fossils, and the background colors represent the PWQ from the model simulations. In the western Tethys region, the PWQ significantly decreased from the Paleocene to the late Eocene, followed by a slight fluctuating increase beginning in the early Oligocene. In the central Tethys region, the arid areas gradually expanded as the Tethys Sea retreated. The eastern Tethys region gradually became more humid with the northward movement of the Indian Plate and the development of the Tibetan Plateau.

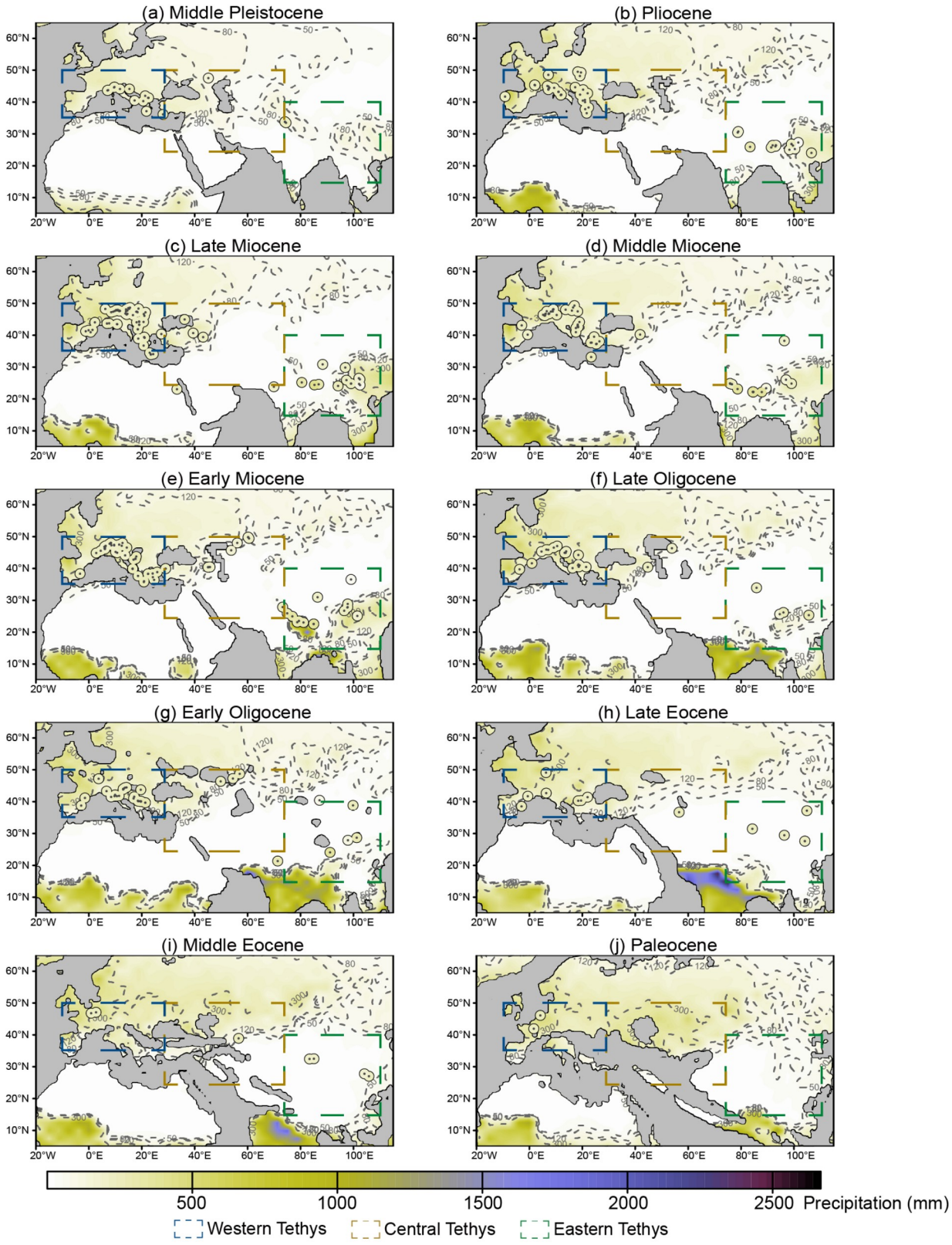

Figure 7 Precipitation in coldest quarter (PCQ) in the Tethys Sea region during the Cenozoic. The circles represent the PCQ reconstructed from fossils, and the background colors represent the PCQ from model simulations. In the western Tethys region, the PCQ did not change significantly, but it experienced a slight fluctuating decreasing trend overall. The central Tethys region began to experience significant aridification during the middle Eocene. The eastern Tethys region was generally arid, however, the precipitation increased in the southeast starting in the late Oligocene, leading to a decrease in the degree of aridity.

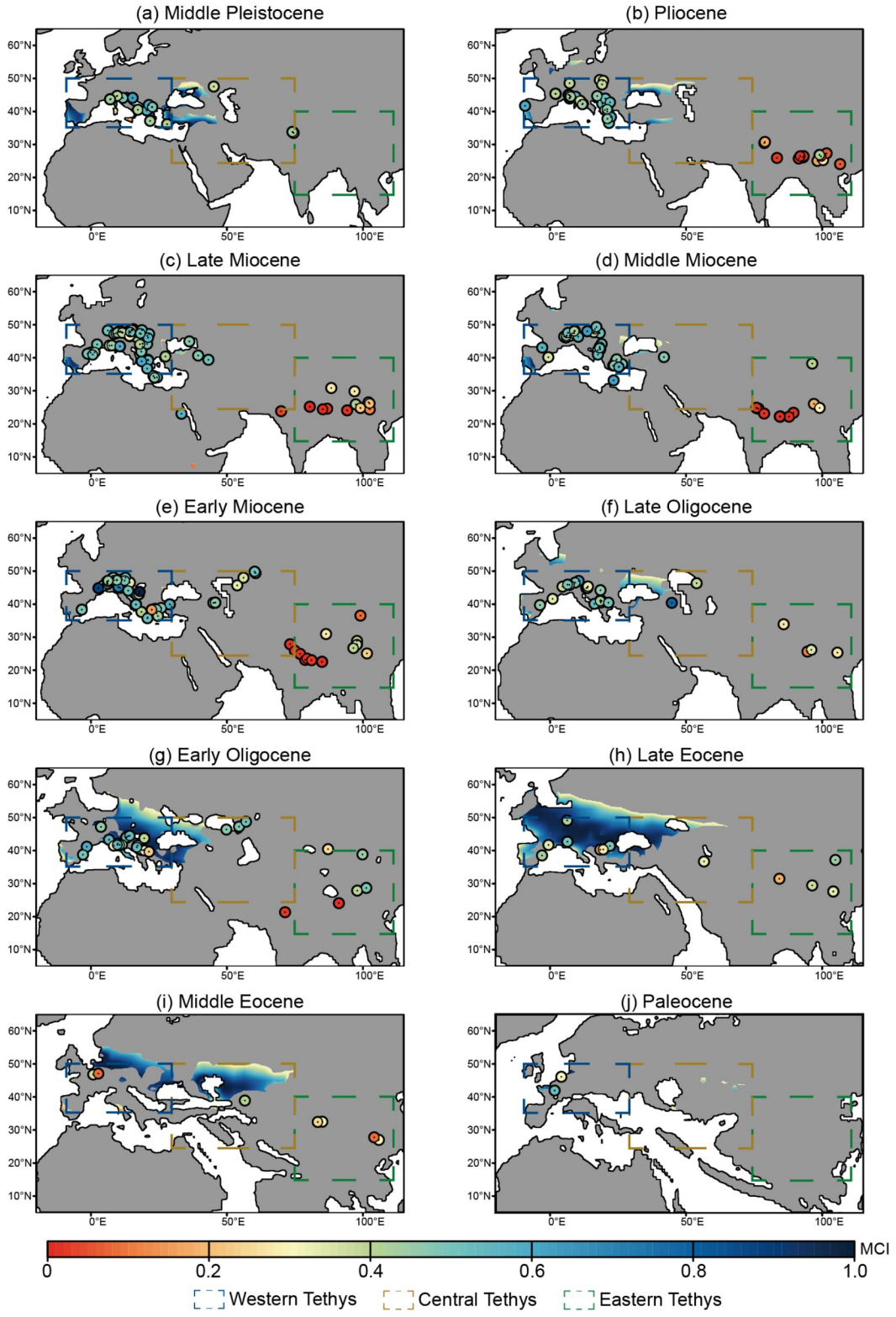

Figure 8 Distribution of the Mediterranean climate in the Tethys Sea region during the Cenozoic. For the MCI, values closer to 1 indicate a higher similarity to the present-day Mediterranean climate type, while values closer to 0 suggest a lower similarity to the Mediterranean climate. The circles represent the MCI reconstructed from fossils, and the background colors represent the MCI from the model simulations. In the western Tethys region, the Mediterranean climate was widely distributed in the middle and high latitude regions during the Eocene. Subsequently, its range began to shrink, became sporadically distributed, and moved toward lower latitudes in the Oligocene. The distribution of the Mediterranean climate was the widest in the central Tethys region during the middle Eocene, and then, it continuously shrank to the Black Sea area. The eastern Tethys region did not experience a Mediterranean climate during the Cenozoic.

portion of land area is consistent with the temperature changes. In the central Tethys region, the temperature changes do not correlate with the proportion of land area or the altitude changes, but they are consistent with the global CO_2 concentration changes. In the eastern Tethys region, temperature exhibits a fluctuating cooling trend during the Paleocene-Quaternary, and there is no correlation with the changes in the proportion of land area. From the Paleocene to the middle Eocene, in the eastern Tethys region, the temperature increases with increasing global CO_2 concentrations, after which its trend is opposite to that of the regional altitude changes.

Overall, the amplitude of the temperature changes in the Tethys region during the Cenozoic reconstructed using the JPDFs method is significantly smaller than that of the model simulation results (Figure 9). The trends of the quantitatively reconstructed MAT, WMMT, and CMMT in the western, central, and eastern Tethys regions are largely consistent. In the western Tethys region, the reconstructed MAT is 9–20°C, the WMMT is 19–26°C, and the CMMT is 0–14°C. For the central Tethys region, the reconstructed MAT is 11–20°C, the WMMT is 20–26°C, and the CMMT is 1–15°C. For the eastern Tethys region, the reconstructed MAT is 11–27°C, the WMMT is 19–30°C, and the CMMT is 1–25°C (Figures 2, 3, 4, and 9). Regarding the fossil reconstruction results, the trends of the MAT, WMMT, and CMMT in the western, central, and eastern Tethys regions in the Cenozoic are consistent (Figure 9h–9j). Among these, the temperature change trends reconstructed from the fossils in the western and central Tethys regions (Figure 9h–9j) are largely consistent with the temperature change trends from the model simulations (Figure 9e–9g), but the amplitude of the change is significantly smaller than that of the model changes. The temperature reconstruction trend for the eastern Tethys region exhibited inconsistencies compared to the model simulation trend.

3.2.2 Precipitation variations

For the model simulations of the western Tethys region in the Cenozoic, the MAP is 600–950 mm, the PWQ is 50–150 mm, and the PCQ is 212.5–290 mm. In the central Tethys region, the MAP is 200–600 mm, the PWQ is 60–150 mm, and the PCQ is 50–200 mm. In the eastern Tethys region, the MAP is 740–1350 mm, the PWQ is 350–690 mm, and the PCQ is 12.5–75 mm. Regarding the trends from the model simulations, in the western Tethys region, during the Cenozoic, the MAP and PCQ trends are similar and inversely related to the trend of the proportion of the land area. Similarly, in the central Tethys region, the trends of the MAP and PCQ are also inversely related to the proportion of the land area. In both the western and central Tethys regions, the trends of the PWQ resemble those of the altitude changes, but the overall changes are not very pronounced. In the eastern Tethys region, during the Cenozoic, the trends of the MAP and PWQ are similar to those of the altitude changes, i.e., fluctuating increasing trends, while the trend of the PCQ is not very noticeable.

Overall, the amplitude of the precipitation changes in the Tethys region during the Cenozoic reconstructed using the JPDFs method is significantly smaller than that of the model simulation results (Figure 10). The quantitatively reconstructed trends of the MAP, PWQ, and PCQ in the western, central, and eastern Tethys regions are largely consistent. The reconstructed MAP in the western Tethys region is 700–1700 mm, the PWQ is 150–520 mm, and the PCQ is 112.5–340 mm. In the central Tethys region, the reconstructed MAP is 600–1500 mm, the PWQ is 150–450 mm, and the PCQ is 100–375 mm. In the eastern Tethys region, the reconstructed MAP is 600–2900 mm, the PWQ is 150–950 mm, and the PCQ is 0–640 mm. Regarding the fossil reconstruction results, the trends of the MAP, PWQ, and PCQ in the western, central, and eastern Tethys regions in the Cenozoic are not pronounced, with very small amplitudes of change. This is particularly obvious for the eastern Tethys precipitation reconstruction results, which differ significantly from the simulation results, with the overall precipitation being much higher than the simulation results.

4. Discussion

4.1 Analysis of regional climate evolution in the Tethys Sea region

According to the results obtained using paleobotanical evidence and model simulations, the modern Mediterranean region experienced a completely humid climate during the Paleogene, during which a large portion of Europe was submerged by seawater, and the PCQ was significantly higher than the PWQ, with a widespread Mediterranean-type climate similar to the present-day climate. According to the simulated winter wind field maps (Appendix 4, Figure S12), during the Paleogene, this region was primarily controlled by the westerlies, which transported abundant moisture from the Atlantic, leading to plentiful PCQ. The atmospheric vertical velocity (Appendix 4, Figure S9) indicates that during summer, the region was primarily dominated by the subtropical high, with descending air currents leading to drier and hotter summers. The global cooling that began in the Oligocene led to a shift toward a semi-humid warm temperate climate. During this time period, the coastal temperatures decreased slightly, the winter precipitation still exceeded summer precipitation, but the difference diminished, and as the Tethys Sea retreated westward, the westerlies also weakened (Appendix 4, Figure S12). Early studies have suggested that the Mediterranean climate first

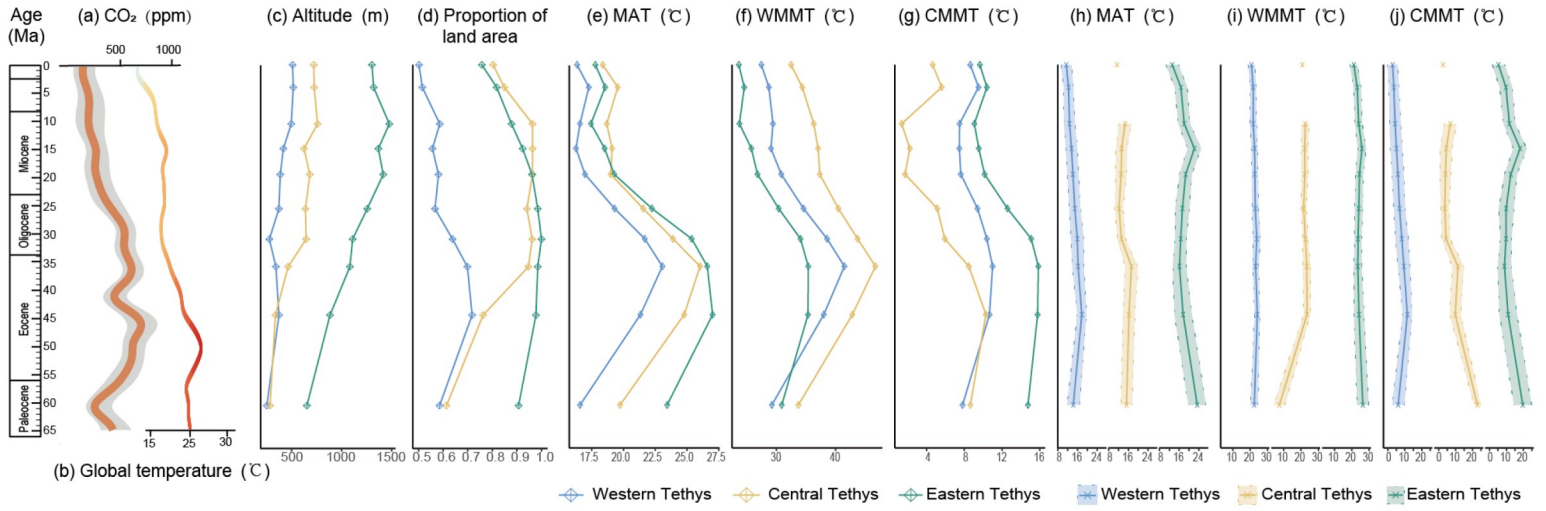

Figure 9 Comparisons of (a) global CO_2 concentration, (b) global temperature, (c) altitude, and (d) proportion of the land area in the Tethys Sea region; (e–g) model-simulated temperatures and (h–j) fossil-reconstructed temperatures. The global CO_2 concentration curve in (a) and the global average surface temperature curve in (b) are adapted from Tierney et al. (2020); the data for the altitude change curve in (c) and the proportion of the land area curve in (d) are sourced from the University of Bristol Research on Initiative for the Dynamic Global Environment (BRIDGE) Earth System Model Simulations website (https://www.paleo.bristol.ac.uk/resources/simulations/).

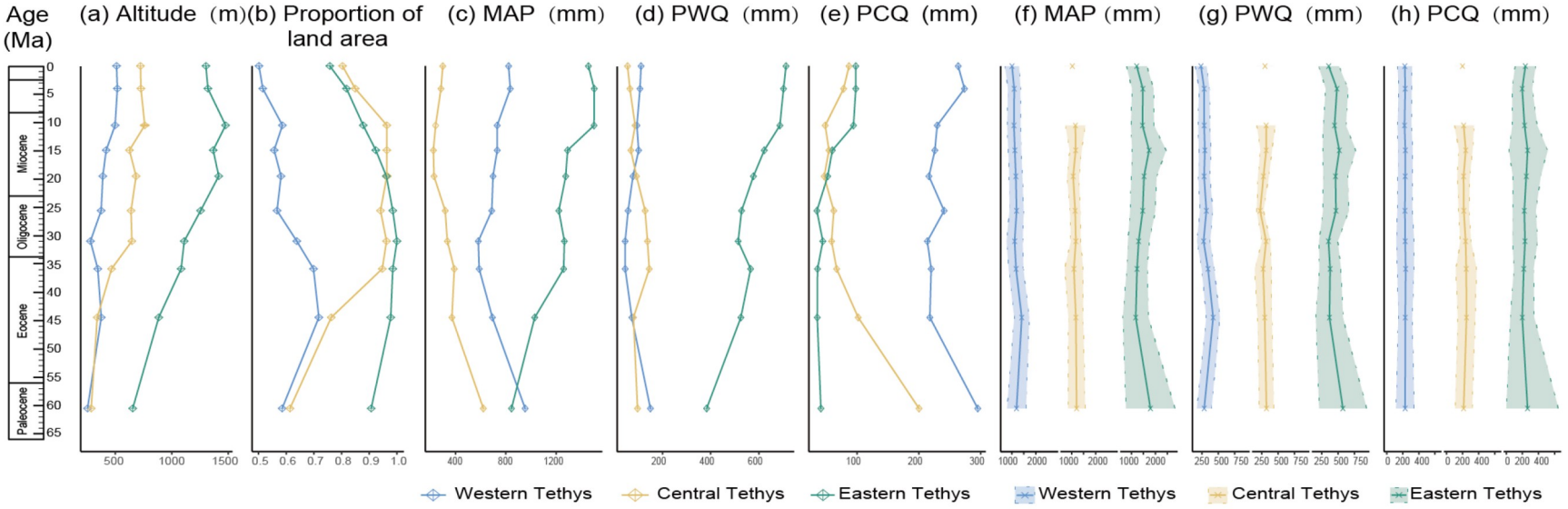

Figure 10 Comparison of (a) the modeled altitude in the Tethyan region, (b) the proportion of the land area, (c–e) the model-simulated precipitation, and (f–h) the fossil-reconstructed precipitation.

emerged during the Pliocene (Suc, 1984). Some studies have suggested that the emergence of the ancient Mediterranean climate can be traced back to the Middle Miocene Climatic Optimum (MMCO), during which the polar atmospheric and oceanic circulations intensified, influencing the development of the Hadley circulation and the seasonal movement of the subtropical high-pressure centers and favoring the formation of a Mediterranean-type climate (Rundel et al., 2016). However, both the simulations and fossil data utilized in this study indicate that during this period, the Mediterranean climate had a very limited distribution, possibly due to high summer precipitation. Based on the simulation results, it is noteworthy that the Mediterranean climate did not exhibit strong seasonal precipitation differences in all regions, as has been previously thought, and some areas may have had weaker seasonal precipitation differences (Rundel et al., 2016). Since the simulation results represent the average precipitation across all of the regions, the difference between the winter and summer precipitation is smaller. The simulation results suggest that the retreat of the Tethys Sea likely altered the distribution of the regional pressure field, affecting the roles of the westerlies and the subtropical high-pressure belt and thereby leading to regional climate changes. Due to the complexity of the region's topography, further high-resolution climate simulations based on more reliable paleogeographic data are necessary.

During the Cenozoic, the collision of the Indian and Eurasian plates, caused the northward compression of the Pamir Plateau, and the global sea level change led to the complex process of the Tethys Sea's withdrawal from Central Asia, which was characterized by repeated transgression-regression cycles (Tang et al., 2011; Sun et al., 2013). The simulation results indicate that from the middle Eocene onwards, Central Asia experienced increasing drought, which coincided with the retreat of the Tethys Sea from the Tarim Basin and the Tajik Basin (Sun and Jiang, 2013; Sun et al., 2016). During the Oligocene, the severity of the drought intensified, and its extent expanded compared to that in the Eocene. The cooling during this time period was potentially driven by global climate trends, the retreat of the Tethys Sea, and decreased water vapor transport due to the development of the Tibetan Plateau, Pamir Plateau, and Tianshan Mountains (Sun et al., 2020). Before the MMCO, the sea retreated from central Iran, resulting in increased aridity and extreme low temperatures (Sun et al., 2021b). Possibly influenced by the MMCO, the arid region in Central Asia contracted slightly during this period. Subsequently, the final closure of the Tethys Sea's northwestern seaway during the Late Miocene may have triggered the expansion of the East Antarctic Ice Sheet, leading to a global drop in sea level and exacerbating aridity in Central Asia (Sun et al., 2021a). From the perspective of the precipitation trend results, the retreat of the Tethys Sea from Central Asia primarily led to a reduction in the PCQ.

Geological evidence highlights the occurrence of significant environmental shifts in China around the transition from the Paleogene to the Neogene. The vast arid belt that extended across eastern and western China during the Paleogene (65–24 Ma) evolved into a northwestern arid and southeastern humid configuration by the Miocene (Wang, 1990; Liu et al., 1998; Sun and Wang, 2005; Guo, 2017; Li et al., 2022). However, there is considerable debate regarding the spatial and temporal extent of this arid belt. Recent analyses suggest that southeastern China experienced a monsoon climate with humid broad-leaved forests during the Eocene, indicating that a combination of monsoon climate, global cooling, and topographic changes drove the vegetation transition from humid forests in the southeast to arid shrublands or open woodlands in the northwest (Li et al., 2022). The precipitation simulation results obtained in this study show that during the Paleogene, the arid belt was seasonally present. In southeastern China, the MAP was around 1300 mm, the PWQ was around 270 mm, and the PCQ was less than 50 mm, indicating the presence of a pronounced arid belt. At the Oligocene-Miocene boundary, the higher PCQ in southeast China, which may have been due to the uplift of the northern Tibetan Plateau, mitigated the arid conditions (Li et al., 2021). Ding et al. (2014) pointed out that during the Paleocene, the high-altitude Gangdise Mountains and the uplifting Himalayas created an arid interior region of the plateau, which is consistent with the simulated precipitation results. The southern Gangdise Mountains had larger amounts of precipitation and a warm and humid climate during the Paleocene, while the interior of the plateau was relatively dry and hot, especially in winter. During the Eocene, a central E-W-oriented valley existed in Xizang, and it was flanked by the Gangdise Mountains to the south and the Qiangtang Mountains to the north. The central valley transitioned from a warm and humid subtropical forest to a drier open woodland during the late Eocene (Zhang et al., 2022). The simulation results indicate that the climate was cooler during this period, with greater PWQ and winter aridity. The simulation results also indicate that at the Eocene-Oligocene boundary, there was a significant increase in precipitation along the southeastern edge of Xizang, which may have been related to the continuous uplift of the region (Su et al., 2019). It is noteworthy that, according to the model simulation results, on the windward slope of the southern edge of the Tibetan Plateau, the MAP and PCQ were not strongest after the formation of the Tibetan Plateau in the Neogene and were instead strongest during the late Eocene to early Oligocene. This may have been related to the higher global CO_2 concentrations during this period. By the Late Miocene, when the Tibetan Plateau had approximately reached its current elevation (Deng and Ding, 2015), the climate of the modern eastern Tethys coastal region had essentially formed.

4.2 Evolutionary process of Mediterranean climate

The simulation results indicate that during the Eocene, the range of the Mediterranean climate expanded continuously, spreading from the middle to high latitudes across Europe in the middle Eocene. During this period, the PCQ decreased slightly, while the PWQ decreased significantly in these regions, which may be the reason for the expansion of the distribution range. Beginning in the early Oligocene, the distribution range of the Mediterranean climate shrank dramatically, particularly in Germany, France, and Spain. The PCQ continued to decrease during the Oligocene, and by the late Miocene, most areas in the western Tethys region had PCQ values of 100–120 mm. During this period, the PWQ fluctuated and increased, and only the Black Sea region, the southern tip of Iberia, and some other peninsulas had PWQ values of around 80 mm, while other regions experienced higher PWQ values of up to 120 mm. The reduction in the seasonal precipitation differences from the Oligocene to the Late Miocene may have been the reason for the sporadic distribution of the Mediterranean climate. Paleobotanical evidence suggests that during the Eocene, Germany still had a subtropical humid climate with evergreen sclerophyllous forest vegetation (Moraweck et al., 2015; Kunzmann et al., 2019). Beginning in the early Oligocene, the climate in Germany shifted to a humid Cfa type with a greater PWQ, which was significantly higher than the PCQ (Utescher et al., 2000; Mach et al., 2014; Kvaček et al., 2020; Müller et al., 2023). This further confirms that the distribution range of the Mediterranean climate was closely related to the PWQ. Although the global climate changed during the Eocene-Oligocene leading to widespread dry and cold climates, the PWQ increased in southern France and northern Spain, resulting in enhanced seasonality and a shift in the vegetation types from moisture-loving and heat-loving vegetation to open savannas (Tosal et al., 2019, 2023). After the Messinian salinity crisis in the Late Miocene, in the western Tethys region, both the PCQ and PWQ increased in the Pliocene. By the Quaternary, the overall PCQ decreased, but in the southern tip of the western Tethys Peninsula and the Black Sea region, the PWQ dropped significantly below 80 mm, and thus, these regions had distinct Mediterranean climates. It can be seen that the distribution of the Mediterranean climate mainly depended on the difference in the seasonal precipitation, especially the degree of summer aridity, which was crucial for the evolution of the Mediterranean climate.

4.3 Relationship between topographic changes and vegetation evolution in the Tethys Sea region

The Eurasian continent, with its vast landmass and proximity to multiple oceans, fosters diverse climate types, which drive plant diversity and evolution. Plants, due to their immobility, continuously adapt to climate changes and thus can serve as proxy indicators for environmental variations (Li et al., 2003; Wang et al., 2009). Tectonic movements and climatic events have shaped the complex topography and diverse climates, making Eurasia home to numerous biodiversity hotspots (Myers et al., 2000; Zhao Z et al., 2022), including the Mediterranean Basin, the Caucasus region, the Iranian-Anatolian Plateau, the mountain ranges in Central Asia, and the Hengduan Mountains-East Himalaya area, all of which are distributed along the Tethys orogenic domain. MAP and PWQ changes may contribute to the high biodiversity and endemism in communities in areas with a Mediterranean climate (Deitch et al., 2017). However, our simulation results show that the temperature and precipitation changes in the western Tethys region were not significant, suggesting that the current climate is not drastically different from the climate in the Paleogene. Compared to the changes in the PCQ, the decreases in the PWQ and MAP were more pronounced. In contrast, the central Tethys region experienced a clear trend of winter cooling and precipitation reduction, while the eastern Tethys area experienced a significant decrease in temperature and an increase in precipitation. Fossil evidence suggests that during the Paleogene, the Tethyan flora was composed of humid and warm subtropical type flora characterized by evergreen shrubs and trees, corresponding to the subtropical warm and humid climate type, which is consistent with our simulation results. However, how the complex topography and climate changes in the Tethyan coastal area during the Cenozoic likely promoted plant diversity evolution and what characteristics the changes in the vegetation types exhibited remain unclear. Investigating these changes is crucial for biodiversity conservation (Olson et al., 2001).

4.4 Comprehensive analysis of model simulation and quantitative reconstruction

The comparison of the quantitative reconstruction of the paleoclimate and model simulations for the Tethys Sea region in the Cenozoic yielded generally consistent results. In terms of temperature, the western and central Tethyan regions experienced a warming trend from the Paleocene to the late Eocene, followed by a cooling trend beginning in the early Oligocene. This corresponds to the global climate changes during the Cenozoic, which were driven by variations in the CO_2 concentration, leading to a greenhouse climate phase from the Paleocene to the Eocene and a cooling period at the Eocene-Oligocene boundary (Westerhold et al., 2020). The eastern Tethyan region, influenced by the rapid development of the Tibetan Plateau, began to cool during the late Eocene (Ding et al., 2014), and the amplitude of the temperature changes was greater in summer than in winter. Due to the screening process, no fossil data from the early

Eocene met the required criteria, and hence, the high temperatures in the early Eocene are not reflected in the results. The model simulations indicate that a peak in temperature occurred at around 35 Ma. We attribute this to the CO_2 concentration settings proposed by Foster et al. (2017), namely, 570–736 ppmv and 901 ppmv in the middle and late Eocene, respectively, resulting in a warmer late Eocene. However, the reconstructed temperatures during the Paleocene-Eocene greenhouse climate period exhibited significant deviations, with the reconstructed temperatures being noticeably colder than the simulated temperatures. The NLRs of the fossil plants were mostly on the genus level, or even the family level, leading to potential biases in the temperature reconstruction (Utescher et al., 2000). Additionally, the temperatures extracted from the NLRs of the plants may also differ from the ecological niches of plants during the Paleogene greenhouse period. Despite all of these potential biases based on the fossil data, the majority of the fossil sites contained more than 20 different plant species, so the JPDFs method, based on a large number of plant species for quantitative reconstruction, can minimize the errors as much as possible. However, the evolutionary process of the plant ecological niches is changeable, and errors in the quantitative paleoclimate reconstruction brought about by changes in the range of ecological niche adaptation are still difficult to completely eliminate to some extent. Moreover, there is a phenomenon of the reconstructed temperatures being too warm on the southern edge of the Tibetan Plateau, which may be related to deviations in the latitudes and longitudes of the fossil sites.

Apart from the Tibetan Plateau region, the overall amplitude of the precipitation changes is relatively minor. In the western Tethyan region, during the Cenozoic, the PWQ changes are not prominent, but there is a decrease in PCQ. The central Tethys region exhibits a clear trend of aridification following topographic changes, while the eastern Tethys region exhibits a fluctuating, increasing precipitation trend, with higher precipitation on the southern edge of the Tibetan Plateau during the late Eocene to the early Oligocene. However, in the central and eastern Tethys regions, where the model simulated arid conditions, the reconstructed precipitation is higher. This discrepancy may be due to the presence of complex micro-terrains in these areas. The model simulations lack high resolution topographic data, which could reduce the accuracy of the simulation of the effects of the local topography and geomorphology on the climate. Overall, the amplitudes of the paleo-temperature and paleo-precipitation changes reconstructed from fossils are not as significant as those of the model simulation results, and there is even an inconsistent trend in the Tibetan Plateau region, which may be affected by the spatial and temporal distributions of the collected fossil sites, especially in the Tibetan Plateau region (Sun et al., 2013). The plant fossils from the study area do not fully capture the climatic evolution of the entire region.

Based on the spatial analysis results of the paleoclimate, although the temperature and precipitation reconstructed from fossil sites in individual regions deviate from the model simulation results, the temperature and precipitation reconstructed from most of the fossil sites are consistent with the model results. The method of reconstructing the paleoclimate using fossils is inevitably influenced to a large extent by factors such as the fossil burial conditions, preservation status, and quantity of fossils. From the perspective of time series changes in the paleoclimate, the climate change trends reconstructed using fossils are not obvious. This may be primarily due to the large differences in the spatial and temporal distributions of the fossil sites. The collected fossil data are largely concentrated in the western Tethys region, followed by the eastern Tethys region, while the central Tethys region has fewer fossil sites due to limitations imposed by the fossil burial conditions. In particular, in Central Asia, most of the fossil sites may be distributed in relatively humid areas, while very few fossil sites are located in arid and semi-arid regions, leading to possible spatial imbalance of the climate reconstruction for this region since the Cenozoic. This could explain the less obvious change trend. There are also significant differences in the number of fossil sites in the same region during the different geological periods in the Cenozoic. Most of the fossil sites are located in Miocene strata, fewer are located in Paleocene and Quaternary strata, and there are even no fossil sites in Quaternary strata in the central Tethys region. Under these conditions, averaging the fossil site data from different regions and periods results in change trends with smaller amplitudes. For scattered fossil site data, model simulations can obtain paleoclimate values for the entire region, they can more intuitively display the changes in the paleoclimate. Therefore, fossil data can provide a more intuitive picture of the climate and vegetation, and model simulations can provide more comprehensive information about climate changes across the entire region. Although there are some deviations between the two methods, cross-validation can provide more reliable evidence for paleoclimate reconstruction on a large regional scale.

Plant fossils do record information about the environment and climate during geological history (Wang et al., 2009). However, there are challenges related to incomplete fossil records and changes in the distribution areas of the NLRs. Model simulations can help address the gaps in geological evidence, but they also face challenges due to the imprecision of boundary conditions, especially regarding topography and geomorphology (Liu, 1993; Ding and Xiong, 2006). Therefore, it is essential to combine both approaches, i.e., to use them to complement and validate each other, in order to achieve a more comprehensive understanding of the

mechanisms of paleoclimate change (Sun, 2014; Zheng et al., 2019).

5. Conclusions

In conclusion, both the quantitative reconstructions using fossils and model simulation results indicate that under the influence of global CO_2 concentration changes, the retreat and closure of the Tethys Sea contributed to the evolution of the Mediterranean climate in the western Tethys region, while the central Tethys region gradually became drier and cooler during the late Oligocene to Early Miocene. Concurrently, during the rapid development of the Tibetan Plateau, the eastern Tethys region experienced fluctuating wetter and colder conditions in the late Oligocene. The Mediterranean climate was prevalent in Central Asia and Europe during the Eocene to early Oligocene, but its distribution range contracted significantly in the Miocene, primarily due to the increase in the PWQ.

Acknowledgements *We thank Jiao MA, Chongtao XU, Peirong CHEN, and Xiaoqi FANG for helping with the data collection. This work was supported by the National Key Research and Development Program of China (Grant No. 2022YFF0800800), the National Natural Science Foundation of China (Grant No. 42372033), the National Science Fund for Distinguished Young Scholars (Grant No. 42425201), the Second Tibetan Plateau Scientific Expedition and Research Program of the Chinese Academy of Sciences (Grant No. 2019QZKK0705), the Yunnan Provincial Reserve Talents Program for Young and Middle-aged Academic and Technical Leaders (Grant No. 202305AC160051), and the Sub-project of the 14th Five-Year Scientific and Technological Innovation Plan of the Xishuangbanna Tropical Botanical Garden, Chinese Academy of Sciences (Grant No. XTBG-1450101).*

Conflict of interest The authors declare that they have no conflict of interest.

References

Aleksandrova A N, Prozorov Y I, Yasamanov N A. 1987. Climatic and floristic zonation of the Mediterranean region during early Cenozoic time. Int Geol Rev, 29: 503–514

Altolaguirre Y, Postigo-Mijarra J M, Casas-Gallego M, Moreno-Domínguez R, Barrón E. 2023. Mapping the late Miocene Pyrenean Forests of the La Cerdanya Basin, Spain. Forests, 14: 1471

An Z S, Zhang P Z, Wang E Q, Wang S M, Qiang X K, Li L, Song Y G, Chang H, Liu X D, Zhou W J, Liu W G, Cao J J, Li X Q, Shen J, Liu Y, Ai L. 2006. Changes of the monsoon-arid environment in China and growth of the Tibetan Plateau since the Miocene (in Chinese with English Abstract). Quat Sci, 26: 678–693

Barrón E, Rivas-Carballo R, Postigo-Mijarra J M, Alcalde-Olivares C, Vieira M, Castro L, Pais J, Valle-Hernández M. 2010. The Cenozoic vegetation of the Iberian Peninsula: A synthesis. Rev Palaeobot Palynol, 162: 382–402

Bertini A, Martinetto E. 2011. Reconstruction of vegetation transects for the Messinian-Piacenzian of Italy by means of comparative analysis of pollen, leaf and carpological records. Palaeogeogr Palaeoclimatol Palaeoecol, 304: 230–246

Bosboom R, Dupont-Nivet G, Grothe A, Brinkhuis H, Villa G, Mandic O, Stoica M, Kouwenhoven T, Huang W T, Yang W, Guo Z J. 2014. Timing, cause and impact of the late Eocene stepwise sea retreat from the Tarim Basin (west China). Palaeogeogr Palaeoclimatol Palaeoecol, 403: 101–118

Bozukov V, Utescher T, Ivanov D. 2009. Late Eocene to early Miocene climate and vegetation of Bulgaria. Rev Palaeobot Palynol, 153: 360–374

Bozukov V, Vatsev M, Ivanov D, Simov N. 2021. New fossil flora from Palaeogene sediments near Bersin village (SW Bulgaria). Rev Bulg Geol Soc, 82: 102–104

Bruch A A, Zhilin S G. 2007. Early Miocene climate of Central Eurasia—Evidence from Aquitanian floras of Kazakhstan. Palaeogeogr Palaeoclimatol Palaeoecol, 248: 32–48

Bubík M, Doláková N, Kvaček Z, Teodoridis V. 2022. A new early Miocene (Ottnangian) flora of the "Rzehakia Beds" from Brno-Líšeň. Fossil Imprint, 78: 263–287

Cai M T, Fang X M, Wu F L, Miao Y F, Appel E. 2012. Pliocene-Pleistocene stepwise drying of Central Asia: Evidence from paleomagnetism and sporopollen record of the deep borehole SG-3 in the western Qaidam Basin, NE Tibetan Plateau. Glob Planet Change, 94-95: 72–81

Carrapa B, DeCelles P G, Wang X, Clementz M T, Mancin N, Stoica M, Kraatz B, Meng J, Abdulov S, Chen F. 2015. Tectono-climatic implications of Eocene Paratethys regression in the Tajik Basin of Central Asia. Earth Planet Sci Lett, 424: 168–178

Collinson M E, Manchester S R, Wilde V. 2012. Fossil fruits and seeds of the middle Eocene Messel biota, Germany. Abh Senckenberg Ges Naturforsch, 570: 1–249

Cox P M. 2001. Description of the TRIFFID dynamic global vegetation model. Technical Report. Exeter, UK: Met Office Hadley Centre

Cox P M, Huntingford C, Harding R J. 1998. A canopy conductance and photosynthesis model for use in a GCM land surface scheme. J Hydrol, 212-213: 79–94

Cox P M, Betts R A, Jones C D, Spall S A, Totterdell I J. 2000. Acceleration of global warming due to carbon-cycle feedbacks in a coupled climate model. Nature, 408: 184–187

Deitch M J, Sapundjieff M J, Feirer S T. 2017. Characterizing precipitation variability and trends in the world's Mediterranean-climate areas. Water, 9: 259

Deng T, Ding L. 2015. Paleoaltimetry reconstructions of the Tibetan Plateau: Progress and contradictions. Natl Sci Rev, 2: 417–437

Denk T, Güner T H, Kvaček Z, Bouchal J M. 2017. The early Miocene flora of Güvem (Central Anatolia, Turkey): A window into early Neogene vegetation and environments in the Eastern Mediterranean. Acta Palaeobot, 57: 237–338

Denk T, Güner H T, Bouchal J M, Kallanxhi M E. 2021. The Pleistocene flora of Bezhan, southeast Albania: Early appearance of extant tree species. Historical Biol, 33: 283–305

Denk T, Sami M, Teodoridis V, Martinetto E. 2022. The late early Pleistocene flora of Oriolo, Faenza (Italy): Assembly of the modern forest biome. Fossil Imprint, 78: 217–262

Ding L, Xu Q, Yue Y H, Wang H Q, Cai F L, Li S. 2014. The Andean-type Gangdese Mountains: Paleoelevation record from the Paleocene-Eocene Linzhou Basin. Earth Planet Sci Lett, 392: 250–264

Ding L, Maksatbek S, Cai F L, Wang H Q, Song P P, Ji W Q, Xu Q, Zhang L Y, Muhammad Q, Upendra B. 2017. Processes of initial collision and suturing between India and Asia. Sci China Earth Sci, 60: 635–651

Ding Z L, Xiong S F. 2006. Numerical modeling in paleoclimate study: Progress and problrms (in Chinese with English Abstract). Earth Sci Front, 13: 21–31

Duggen S, Hoernle K, van den Bogaard P, Rüpke L, Phipps Morgan J. 2003. Deep roots of the Messinian salinity crisis. Nature, 422: 602–606

Edwards E J, Osborne C P, Strömberg C A E, Smith S A, Bond W J, Christin P A, Cousins A B, Duvall M R, Fox D L, Freckleton R P, Ghannoum O, Hartwell J, Huang Y, Janis C M, Keeley J E, Kellogg E A, Knapp A K, Leakey A D B, Nelson D M, Saarela J M, Sage R F, Sala O E, Salamin N, Still C J, Tipple B. 2010. The origins of C_4

grasslands: Integrating evolutionary and ecosystem science. Science, 328: 587–591
Erdei B, Wilde V. 2020. The Eocene flora of Tatabánya “marl-mine” (N Hungary). Palaeobio Palaeoenv, 100: 629–645
Erdei B, Utescher T, Hably L, Tamás J, Roth-Nebelsick A, Grein M. 2012. Early Oligocene continental climate of the Palaeogene basin (Hungary and Slovenia) and the surrounding area. Turkish J Earth Sci, 21: 153–186
Erdei B, Hably L, Héja G, Fodor L. 2022. The late Oligocene macroflora of Zsámbék, central Hungary. Fossil Imprint, 78: 298–309
Fenton I S, Aze T, Farnsworth A, Valdes P, Saupe E E. 2023. Origination of the modern-style diversity gradient 15 million years ago. Nature, 614: 708–712
Foster G L, Royer D L, Lunt D J. 2017. Future climate forcing potentially without precedent in the last 420 million years. Nat Commun, 8: 14845
Garcia-Castellanos D, Villaseñor A. 2011. Messinian salinity crisis regulated by competing tectonics and erosion at the Gibraltar arc. Nature, 480: 359–363
Garcia-Castellanos D, Estrada F, Jiménez-Munt I, Gorini C, Fernàndez M, Vergés J, De Vicente R. 2009. Catastrophic flood of the Mediterranean after the Messinian salinity crisis. Nature, 462: 778–781
Gregor H J. 1990. Contributions to the late Neogene and early Quaternary floral history of the Mediterranean. Rev Palaeobot Palynol, 62: 309–338
Guo Z T. 2017. Loess Plateau attests to the onsets of monsoon and deserts (in Chinese). Sci Sin Terr, 47: 421–437
Hably L. 2010. The early Oligocene flora of Santa Giustina (Liguria, Italy)—Revision and comparison with the flora of the Tard Clay Formation. Riv Ital Paleontol Stratigr, 116: 405–420
Hably L. 2020. The Karpatian (late early Miocene) flora of the Mecsek area. Acta Palaeobotanica, 60: 51–122
Hamon N, Sepulchre P, Lefebvre V, Ramstein G. 2013. The role of eastern Tethys seaway closure in the Middle Miocene climatic transition (ca. 14 Ma). Clim Past, 9: 2687–2702
Hernández-Molina F J, Stow D A V, Alvarez-Zarikian C A, Acton G, Bahr A, Balestra B, Ducassou E, Flood R, Flores J A, Furota S, Grunert P, Hodell D, Jimenez-Espejo F, Kim J K, Krissek L, Kuroda J, Li B, Llave E, Lofi J, Lourens L, Miller M, Nanayama F, Nishida N, Richter C, Roque C, Pereira H, Sanchez Goñi M F, Sierro F J, Singh A D, Sloss C, Takashimizu Y, Tzanova A, Voelker A, Williams T, Xuan C. 2014. Onset of Mediterranean outflow into the North Atlantic. Science, 344: 1244–1250
Huang J, Su T, Li S F, Wu F X, Deng T, Zhou Z K. 2020. Late Miocene vegetation and paleoenvironment of the Zhada Basin, Tibet. Sci China Earth Sci, 50: 220–232
Jin J H, Liao W B, Wang B S, Peng S L. 2003. Global change in Cenozoic and evolution of flora in China (in Chinese with English Abstract). Guihaia, 23: 217–225
Jolly-Saad M C, Pastre J F, Nomade S. 2020. The Zanclean palaeofloras around the Mont-Dore strato-volcano: A window into upper Neogene vegetation and environments in the Massif Central (Puy de Dome, France). Geobios, 59: 29–46
Kafetzidou A, Kouli K, Zidianakis G, Kostopoulos D S, Zouros N. 2022. The early Miocene angiosperm flora of Akrocheiras in Lesvos Petrified Forest (North Aegean, Greece)—Preliminary results. Rev Palaeobot Palynol, 296: 104559
Karger D N, Conrad O, Böhner J, Kawohl T, Kreft H, Soria-Auza R W, Zimmermann N E, Linder H P, Kessler M. 2017. Climatologies at high resolution for the Earth’s land surface areas. Sci Data, 4: 170122
Kayseri-Özer M S. 2017. Cenozoic vegetation and climate change in Anatolia—A study based on the IPR-vegetation analysis. Palaeogeogr Palaeoclimatol Palaeoecol, 467: 37–68
Khan M A, Mahato S, Spicer R A, Spicer T E V, Ali A, Hazra T, Bera S. 2023. Siwalik plant megafossil diversity in the Eastern Himalayas: A review. Plant Divers, 45: 243–264
Kiehl J T, Shields C A. 2013. Sensitivity of the Palaeocene-Eocene thermal maximum climate to cloud properties. Phil Trans R Soc A, 371: 20130093
Kottek M, Grieser J, Beck C, Rudolf B, Rubel F. 2006. World Map of the Köppen-Geiger climate classification updated. Meteorol Z, 15: 259–263
Krijgsman W, Hilgen F J, Raffi I, Sierro F J, Wilson D S. 1999. Chronology, causes and progression of the Messinian salinity crisis. Nature, 400: 652–655
Kunzmann L, Moraweck K, Müller C, Schröder I, Wappler T, Grein M, Roth-Nebelsick A. 2019. A Paleogene leaf flora (Profen, Sachsen-Anhalt, Germany) and its potentials for palaeoecological and palaeoclimate reconstructions. Flora, 254: 71–87
Kutiel H, Trigo R M. 2014. The rainfall regime in Lisbon in the last 150 years. Theor Appl Climatol, 118: 387–403
Kutiel H, Türkeş M. 2017. Spatial and temporal variability of dryness characteristics in Turkey. Int J Climatol, 37: 818–828
Kvaček Z, Bubík M. 2016. A new Oligocene leaf assemblage from the Ghalandar area (NW Iran) and its contribution to understanding of floristic evolution in the eastern Paratethys. Bull Geosci, 91: 705–715
Kvaček Z, Teodoridis V, Radoň M. 2018. Review of the late Oligocene flora of Matrý Near Sebuzín (České Středohoří Mts., the Czech Republic). Fossil Imprint, 74: 292–316
Kvaček Z, Teodoridis V, Denk T. 2020. The Pliocene flora of Frankfurt am Main, Germany: Taxonomy, palaeoenvironments and biogeographic affinities. Palaeobio Palaeoenv, 100: 647–703
Li C S, Wang Y F, Sun Q G. 2003. The quantitative reconstruction of palaeoenvironments and palaeoclimates based on plants (in Chinese with English Abstract). Chin Bull Botany, 20: 430–438
Li J J. 1999. Studies on the geomorphological evolution of the Qinghai-Xizang (Tibetan) Plateau and Asian monsoon (in Chinese with English Abstract). Mar Geol Quat Geol, 19: 7–17
Li Q J, Utescher T, Liu Y S C, Ferguson D, Jia H, Quan C. 2022. Monsoonal climate of East Asia in Eocene times inferred from an analysis of plant functional types. Palaeogeogr Palaeoclimatol Palaeoecol, 601: 111138
Li S F, Mao L M, Spicer R A, Lebreton-Anberrée J, Su T, Sun M, Zhou Z K. 2015. Late Miocene vegetation dynamics under monsoonal climate in southwestern China. Palaeogeogr Palaeoclimatol Palaeoecol, 425: 14–40
Li S F, Xing Y W, Valdes P J, Huang Y J, Su T, Farnsworth A, Lunt D J, Tang H, Kennedy A T, Zhou Z K. 2018. Oligocene climate signals and forcings in Eurasia revealed by plant macrofossil and modelling results. Gondwana Res, 61: 115–127
Li S F, Valdes P J, Farnsworth A, Davies-Barnard T, Su T, Lunt D J, Spicer R A, Liu J, Deng W Y D, Huang J, Tang H, Ridgwell A, Chen L L, Zhou Z K. 2021. Orographic evolution of northern Tibet shaped vegetation and plant diversity in eastern Asia. Sci Adv, 7: eabc7741
Lionello P, Malanotte-Rizzoli F, Boscolo R, Alpert P, Artale V, Li L, Luterbacher J, May W, Trigo R, Tsimplis M, Ulbrich U, Xoplaki E. 2006. The Mediterranean climate: an overview of the main characteristics and issues. Dev Earh Environ Sci, 4: 1–26
Liu D S, Zheng M P, Guo Z T. 1998. Initiation and evolution of the Asian monsoon system timely coupled with the ice-sheet growth and the tectonic movements in Asia (in Chinese with English Abstract). Quat Sci, 18: 194–204
Liu H G, Li S Q, Ugolini A, Momtazi F, Hou Z E. 2018. Tethyan closure drove tropical marine biodiversity: Vicariant diversification of intertidal crustaceans. J Biogeogr, 45: 941–951
Liu X D. 1993. Application of numerical simulation to paleoclimatic research (in Chinese with English Abstract). Sci Geogr Sin, 13: 257–267
Macaluso L, Martinetto E, Vigna B, Bertini A, Cilia A, Teodoridis V, Kvaček Z. 2018. Palaeofloral and stratigraphic context of a new fossil forest from the Pliocene of NW Italy. Rev Palaeobot Palynol, 248: 15–33
Mach K, Teodoridis V, Grygar T M, Kvaek Z, Suhr P, Standke G. 2014. An evaluation of palaeogeography and palaeoecology in the Most Basin (Czech Republic) and Saxony (Germany) from the late Oligocene to the early Miocene. N Jb Geol Paläont Abh, 272: 13–45
Moraweck K, Uhl D, Kunzmann L. 2015. Estimation of late Eocene

(Bartonian-Priabonian) terrestrial palaeoclimate: Contributions from megafloral assemblages from central Germany. Palaeogeogr Palaeoclimatol Palaeoecol, 433: 247–258
Mosbrugger V, Utescher T. 1997. The coexistence approach—A method for quantitative reconstructions of Tertiary terrestrial palaeoclimate data using plant fossils. Palaeogeogr Palaeoclimatol Palaeoecol, 134: 61–86
Müller C, Toumoulin A, Böttcher H, Roth-Nebelsick A, Wappler T, Kunzmann L. 2023. An integrated leaf trait analysis of two Paleogene leaf floras. PeerJ, 11: e15140
Myers N, Mittermeier R A, Mittermeier C G, da Fonseca G A B, Kent J. 2000. Biodiversity hotspots for conservation priorities. Nature, 403: 853–858
Olson D M, Dinerstein E, Wikramanayake E D, Burgess N D, Powell G V N, Underwood E C, D'amico J A, Itoua I, Strand H E, Morrison J C, Loucks C J, Allnutt T F, Ricketts T H, Kura Y, Lamoreux J F, Wettengel W W, Hedao P, Kassem K R. 2001. Terrestrial ecoregions of the world: A new map of life on Earth: A new global map of terrestrial ecoregions provides an innovative tool for conserving biodiversity. Bioscience, 51: 933–938
Popova S, Utescher T, Gromyko D V, Bruch A A, Henrot A J, Mosbrugger V. 2017. Cenozoic vegetation gradients in the mid- and higher latitudes of Central Eurasia and climatic implications. Palaeogeogr Palaeoclimatol Palaeoecol, 467: 69–82
Postigo-Mijarra J M, Barrón E, Gómez Manzaneque F, Morla C. 2009. Floristic changes in the Iberian Peninsula and Balearic Islands (southwest Europe) during the Cenozoic. J Biogeogr, 36: 2025–2043
Postigo-Mijarra J M, Altolaguirre Y, Moreno-Domínguez R, Barrón E, Casas-Gallego M. 2022. Climatic reconstruction at the early Miocene La Rinconada mine (Ribesalbes-Alcora Basin, eastern Spain) based on coexistence approach, CLAMP and LMA analysis. Rev Palaeobot Palynol, 304: 104714
Ramstein G, Fluteau F, Besse J, Joussaume S. 1997. Effect of orogeny, plate motion and land-sea distribution on Eurasian climate change over the past 30 million years. Nature, 386: 788–795
Rundel P W, Arroyo M T K, Cowling R M, Keeley J E, Lamont B B, Vargas P. 2016. Mediterranean biomes: Evolution of their vegetation, floras, and climate. Annu Rev Ecol Evol Syst, 47: 383–407
Sagoo N, Valdes P, Flecker R, Gregoire L J. 2013. The early Eocene equable climate problem: Can perturbations of climate model parameters identify possible solutions? Phil Trans R Soc A, 371: 20130123
Scotese C R. 2016. Tutorial: PALEOMAP PaleoAtlas for GPlates and the PaleoData plotter program. PALEOMAP Project
Serkan Akkiraz M, Nazik A, Özgen-Erdem N, Duygu Durak S. 2022. First micropalaeontological record from the early and middle Eocene Mamuca Formation of the Dümrek Basin, western Central Anatolia, Turkey: Biostratigraphy, depositional history and palaeoclimate. J Asian Earth Sci, 224: 105036
Su T, Xing Y W, Liu Y S C, Jacques F M B, Chen W Y, Huang Y J, Zhou Z K. 2010. Leaf margin analysis: A new equation from humid to mesic forests in China. PALAIOS, 25: 234–238
Su T, Spicer R A, Li S H, Xu H, Huang J, Sherlock S, Huang Y J, Li S F, Wang L, Jia L B, Deng W Y D, Liu J, Deng C L, Zhang S T, Valdes P J, Zhou Z K. 2019. Uplift, climate and biotic changes at the Eocene-Oligocene transition in south-eastern Tibet. Natl Sci Rev, 6: 495–504
Su T, Spicer R A, Wu F X, Farnsworth A, Huang J, Del Rio C, Deng T, Ding L, Deng W Y D, Huang Y J, Hughes A, Jia L B, Jin J H, Li S F, Liang S Q, Liu J, Liu X Y, Sherlock S, Spicer T, Srivastava G, Tang H, Valdes P, Wang T X, Widdowson M, Wu M X, Xing Y W, Xu C L, Yang J, Zhang C, Zhang S T, Zhang X W, Zhao F, Zhou Z K. 2020. A middle Eocene lowland humid subtropical "Shangri-La" ecosystem in central Tibet. Proc Natl Acad Sci USA, 117: 32989–32995
Suc J P. 1984. Origin and evolution of the Mediterranean vegetation and climate in Europe. Nature, 307: 429–432
Sun D H, Wang X, Li B F, Chen F H, Wang F, Li Z J, Liang B Q, Ma Z W. 2013. Evolution of Cenozoic Tethys and its environmental effects on inland drought (in Chinese with English Abstract). Mar Geol & Quat Geol, 33: 135–151
Sun J M. 2014. Case study based on Earth system science theory-geomorphic, environmental, and climatic effects of the tectonic uplift of the Tibetan Plateau. Acta Sci Nat Sunyatseni, 53: 1–9
Sun J M, Jiang M S. 2013. Eocene seawater retreat from the southwest Tarim Basin and implications for early Cenozoic tectonic evolution in the Pamir Plateau. Tectonophysics, 588: 27–38
Sun J M, Windley B F, Zhang Z L, Fu B H, Li S H. 2016. Diachronous seawater retreat from the southwestern margin of the Tarim Basin in the late Eocene. J Asian Earth Sci, 116: 222–231
Sun J M, Zhang Z L, Cao M M, Windley B F, Tian S C, Sha J, Abdulov S, Gadoev M, Oimahmadov I. 2020. Timing of seawater retreat from proto-Paratethys, sedimentary provenance, and tectonic rotations in the late Eocene-early Oligocene in the Tajik Basin, Central Asia. Palaeogeogr Palaeoclimatol Palaeoecol, 545: 109657
Sun J M, Sheykh M, Ahmadi N, Cao M M, Zhang Z L, Tian S C, Sha J G, Jian Z M, Windley B F, Talebian M. 2021a. Permanent closure of the Tethyan seaway in the northwestern Iranian Plateau driven by cyclic sea-level fluctuations in the late middle Miocene. Palaeogeogr Palaeoclimatol Palaeoecol, 564: 110172
Sun J M, Talebian M, Jin C S, Liu W G, Zhang Z L, Cao M M, Windley B F, Sheykh M, Shahbazi R, Tian S C. 2021b. Timing and forcing mechanism of the final Neotethys seawater retreat from Central Iran in response to the Arabia-Asia collision in the late early Miocene. Glob Planet Change, 197: 103395
Sun J M, Sha J G, Wang S Q. 2024. Stepwise closure of the Tethyan seaway and its impact on the Earth's multi-sphere interactions during the Cenozoic (in Chinese). Chin Sci Bull, 69: 184–199
Sun X J, Wang P X. 2005. How old is the Asian monsoon system?—Palaeobotanical records from China. Palaeogeogr Palaeoclimatol Palaeoecol, 222: 181–222
Sun Y B, Yin Q Z, Crucifix M, Clemens S C, Araya-Melo P, Liu W G, Qiang X K, Liu Q S, Zhao H, Liang L J, Chen H Y, Li Y, Zhang L, Dong G C, Li M, Zhou W J, Berger A, An Z S. 2019. Diverse manifestations of the mid-Pleistocene climate transition. Nat Commun, 10: 352
Sun Y Y, Liang Y, Liu H, Liu J, Ji J L, Ke X, Liu X B, He Y X, Wang H Y, Zhang B, Zhang Y S, Zhuang G S, Pei J L, Li Y X, Quan C, Li J X, Aitchison J C, Liu W G, Liu Z H. 2023. Mid-Miocene sea level altitude of the Qaidam Basin, northern Tibetan Plateau. Commun Earth Environ, 4: 3
Tang Z H, Ding Z L, White P D, Dong X X, Ji J L, Jiang H C, Luo P, Wang X. 2011. Late Cenozoic central Asian drying inferred from a palynological record from the northern Tian Shan. Earth Planet Sci Lett, 302: 439–447
Tanrattana M, Boura A, Jacques F M B, Villier L, Fournier F, Enguehard A, Cardonnet S, Voland G, Garcia A, Chaouch S, De Franceschi D. 2020. Climatic evolution in Western Europe during the Cenozoic: Insights from historical collections using leaf physiognomy. Geodiversitas, 42: 151
Teodoridis V, Kvaček Z, Sami M, Utescher T, Martinetto E. 2015. Palaeoenvironmental analysis of the Messinian macrofossil floras of Tossignano and Monte Tondo (Vena del Gesso Basin, Romagna Apennines, Northern Italy). Acta Mus Nat Pragae, Ser B Hist Nat, 71: 249–292
Thiel C, Klotz S, Uhl D. 2012. Palaeoclimate estimates for selected leaf floras from the late Pliocene (Reuverian) of Central Europe based on different palaeobotanical techniques. Turkish J Earth Sci, 21: 263–287
Tierney J E, Poulsen C J, Montañez I P, Bhattacharya T, Feng R, Ford H L, Hönisch B, Inglis G N, Petersen S V, Sagoo N, Tabor C R, Thirumalai K, Zhu J, Burls N J, Foster G L, Goddéris Y, Huber B T, Ivany L C, Kirtland Turner S, Lunt D J, McElwain J C, Mills B J W, Otto-Bliesner B L, Ridgwell A, Zhang Y G. 2020. Past climates inform our future. Science, 370: eaay3701
Tosal A, Valero L, Sanjuan J, Martín-Closas C. 2019. Influence of short- and long-term climatic cycles on floristic change across the Eocene-Oligocene boundary in the Ebro Basin (Catalonia, Spain). Comptes Rendus Palevol, 18: 925–947

Tosal A, Verduzco O, Martín-Closas C. 2021. CLAMP-based palaeoclimatic analysis of the late Miocene (Tortonian) flora from La Cerdanya Basin of Catalonia, Spain, and an estimation of the palaeoaltitude of the eastern Pyrenees. Palaeogeogr Palaeoclimatol Palaeoecol, 564: 110186
Tosal A, Tanrattana M, Fournier F, De Franceschi D, Del Rio C, Martín-Closas C, Lettéron A, Semmani N, Boura A. 2023. Plant palaeoecology of the latest Eocene flora from the Saint-Chaptes and Alès Basins of Gard, southern France. Palaeogeogr Palaeoclimatol Palaeoecol, 627: 111740
Traiser C, Klotz S, Uhl D, Mosbrugger V. 2005. Environmental signals from leaves—A physiognomic analysis of European vegetation. New Phytol, 166: 465–484
Utescher T, Mosbrugger V, Ashraf A R. 2000. Terrestrial climate evolution in northwest Germany over the last 25 million years. PALAIOS, 15: 430–449
Utescher T, Bruch A A, Erdei B, François L, Ivanov D, Jacques F M B, Kern A K, Liu Y S C, Mosbrugger V, Spicer R A. 2014. The coexistence approach—Theoretical background and practical considerations of using plant fossils for climate quantification. Palaeogeogr Palaeoclimatol Palaeoecol, 410: 58–73
Valdes P J, Armstrong E, Badger M P S, Bradshaw C D, Bragg F, Crucifix M, Davies-Barnard T, Day J J, Farnsworth A, Gordon C, Hopcroft P O, Kennedy A T, Lord N S, Lunt D J, Marzocchi A, Parry L M, Pope V, Roberts W H G, Stone E J, Tourte G J L, Williams J H T. 2017. The BRIDGE HadCM3 family of climate models: HadCM3@Bristol v1.0. Geosci Model Dev, 10: 3715–3743
Valdes P J, Scotese C R, Lunt D J. 2021. Deep ocean temperatures through time. Clim Past, 17: 1483–1506
Velitzelos D, Bouchal J M, Denk T. 2014. Review of the Cenozoic floras and vegetation of Greece. Rev Palaeobot Palynol, 204: 56–117
Wang F Y, Yang J, Xu J X, Zhao L C, Jiang H E, Cheng Y M, Yi T M, Wang Q, Ma Q W, Yao Y F. 2009. Research and highlights on the evolution of Cenozoic plants and the reconstruction of palaeoclimate and palaeoenvironments in China (in Chinese with English Abstract). Acta Palaeontol Sin, 48: 569–576
Wang P X. 1990. Neogene stratigraphy and paleoenvironments of China. Palaeogeogr Palaeoclimatol Palaeoecol, 77: 315–334
Wang X, Kraatz B, Meng J, Carrapa B, Decelles P, Clementz M, Abdulov S, Chen F H. 2016. Central Asian aridification during the late Eocene to early Miocene inferred from preliminary study of shallow marine-eolian sedimentary rocks from northeastern Tajik Basin. Sci China Earth Sci, 59: 1242–1257
Westerhold T, Marwan N, Drury A J, Liebrand D, Agnini C, Anagnostou E, Barnet J S K, Bohaty S M, De Vleeschouwer D, Florindo F, Frederichs T, Hodell D A, Holbourn A E, Kroon D, Lauretano V, Littler K, Lourens L J, Lyle M, Pälike H, Röhl U, Tian J, Wilkens R H, Wilson P A, Zachos J C. 2020. An astronomically dated record of Earth's climate and its predictability over the last 66 million years. Science, 369: 1383–1387
Wilf P. 1997. When are leaves good thermometers? A new case for Leaf Margin Analysis. Paleobiology, 23: 373–390
Willard D A, Donders T H, Reichgelt T, Greenwood D R, Sangiorgi F, Peterse F, Nierop K G J, Frieling J, Schouten S, Sluijs A. 2019. Arctic vegetation, temperature, and hydrology during early Eocene transient global warming events. Glob Planet Change, 178: 139–152
Worobiec G, Worobiec E. 2019. Wetland vegetation from the Miocene deposits of the Bełchatów Lignite Mine (central Poland). Palaeontol Electron, 22: 1–38
Worobiec G, Jach R, Machaniec E, Uchman A, Worobiec E. 2015. Eocene flora and trace fossils from the Hruby Regiel section in the Tatra Mountains (Poland): Taxonomic revision of the Wiktor Kuźniar fossil plant collection. Acta Geol Pol, 65: 215–238
Wu F Y, Wan B, Zhao L, Xiao W J, Zhu R X. 2020. Tethyan geodynamics (in Chinese with English Abstract). Acta Petrol Sin, 36: 1627–1674
Xing Y W, Gandolfo M A, Onstein R E, Cantrill D J, Jacobs B F, Jordan G J, Lee D E, Popova S, Srivastava R, Su T, Vikulin S V, Yabe A, Linder H P. 2016. Testing the biases in the rich Cenozoic angiosperm macrofossil record. Int J Plant Sci, 177: 371–388
Yang J, Wang Y F, Spicer R A, Mosbrugger V, Li C S, Sun Q G. 2007. Climatic reconstruction at the Miocene Shanwang Basin, China, using leaf margin analysis, CLAMP, coexistence approach, and overlapping distribution analysis. Am J Bot, 94: 599–608
Yang J, Spicer R A, Spicer T E V, Li C S. 2011. 'CLAMP Online': A new web-based palaeoclimate tool and its application to the terrestrial Paleogene and Neogene of North America. Palaeobio Palaeoenv, 91: 163–183
Zhang R, Jiang D B, Zhang Z S, Zhang C X. 2021. Effects of Tibetan Plateau growth, Paratethys Sea retreat and global cooling on the East Asian climate by the early Miocene. Geochem Geophys Geosyst, 22: e2021GC009655
Zhang X W, Gélin U, Spicer R A, Wu F X, Farnsworth A, Chen P R, Del Rio C, Li S F, Liu J, Huang J, Spicer T E V, Tomlinson K W, Valdes P J, Xu X T, Zhang S T, Deng T, Zhou Z K, Su T. 2022. Rapid Eocene diversification of spiny plants in subtropical woodlands of central Tibet. Nat Commun, 13: 3787
Zhang Z S, Wang H J, Guo Z T, Jiang D B. 2007. What triggers the transition of palaeoenvironmental patterns in China, the Tibetan Plateau uplift or the Paratethys Sea retreat? Palaeogeogr Palaeoclimatol Palaeoecol, 245: 317–331
Zhao C Y, Xiong Z Y, Farnsworth A, Spicer R A, He S L, Wang C, Zeng D, Cai F L, Wang H Q, Tian X L, Valdes P J, Lamu C, Xie J, Yue Y H, Ding L. 2023. The late Eocene rise of SE Tibet formed an Asian 'Mediterranean' climate. Glob Planet Change, 231: 104313
Zhao J G, Li S F, Farnsworth A, Valdes P J, Reichgelt T, Chen L L, Zhou Z K, Su T. 2022. The Paleogene to Neogene climate evolution and driving factors on the Qinghai-Tibetan Plateau. Sci China Earth Sci, 65: 1339–1352
Zhao Z, Hou Z E, Li S Q. 2022. Cenozoic Tethyan changes dominated Eurasian animal evolution and diversity patterns. Zool Res, 43: 3–13
Zheng D, Yao T D. 2006. Uplifting of Tibetan Plateau with its environmental effects (in Chinese with English Abstract). Adv Earth Sci, 21: 451–458
Zheng H B, Guo Z T, Deng T. 2014. Evolution of topography, drainage and biogeograohy in East Asia during the Cenozoic: Summary of the third conference on Earth system science (in Chinese with English Abstract). 2014. Adv Earth Sci, 29: 1280–1286
Zheng W P, Man W M, Sun Y, Liang Y H. 2019. Short commentary on CMIP6 Paleoclimate Modelling Intercomparison Project Phase 4 (PMIP4) (in Chinese with English Abstract). Clim Change Res, 15: 510–518
Zhu R X, Zhao P, Zhao L. 2022. Tectonic evolution and geodynamics of the Neo-Tethys Ocean. Sci China Earth Sci, 65: 1–24

(Editorial handling: Xiaodong LIU)